The FEBS Journal

FEBS PRESS science publishing by scientists

Familial mutations modulate α-synuclein interactions with key neuronal membrane lipids

Abid Ali, Mikhail Matveyenka and Dmitry Kurouski

Department of Biochemistry and Biophysics, Texas A&M University, College Station, TX, USA

Keywords
α-Synuclein; cholesterol; fibrils; phosphatidylcholine; sphingomyelin; toxicity

Correspondence
Dmitry Kurouski, Department of Biochemistry and Biophysics, Texas A&M University, College Station, TX 77843, USA
Tel: +979-458-3448
E-mail: dkurouski@tamu.edu

(Received 12 May 2025, revised 28 July 2025, accepted 1 December 2025)

doi:10.1111/febs.70363

Progressive aggregation of α-synuclein (α-Syn) in the midbrain, hypothalamus and thalamus is linked to Parkinson's disease (PD), one of the fastest growing neurodegenerative diseases in the U.S. Studies of families with PD history revealed several mutations that are responsible for the early-onset (A30P, E46K, A53T) and late-onset (H50Q) forms of PD. A growing body of evidence indicates that phospho-/sphingolipids and cholesterol alter the aggregation properties of wild-type (WT) α-syn. However, the effects of these lipids on the rate of α-syn mutants remain unclear. In the current study, we determined the aggregation rates of A30P, E46K, A53T, H50Q and WT α-syn in the presence of large unilamellar vesicles composed of phosphatidylcholine (PC), sphingomyelin (SM) and cholesterol (Cho)—the key lipids of neuronal membranes. We also utilised a set of biophysical methods to reveal the extent to which lipids alter the morphology and secondary structure of amyloid fibrils. We found that familial mutations uniquely altered α-syn interactions with lipid bilayers, which resulted in the altered rate of protein aggregation in the presence of lipid bilayers. Furthermore, A30P mutation fully disabled α-syn interaction with LUVs, while E46K, A53T and H50Q mutations altered cytotoxicity of α-syn fibrils formed in the presence of lipid bilayers. These results suggest that changes in plasma membrane lipid profiles may have a strong effect on the onset and progression of PD in individuals with familial mutations.

Introduction

Lewy bodies (LBs) are intraneuronal inclusions observed in midbrain, hypothalamus and thalamus of patients diagnosed by Parkinson's disease (PD) [1–3]. This pathology affects over 90,000 people in the U.S. alone with combined direct and indirect costs reaching $52 billion per year [4]. Microscopic analysis of LBs revealed the presence of lipid bilayers and α-synuclein (α-syn) fibrils [5–8]. Numerous in vitro studies demonstrated that lipid membranes could alter the rate of α-syn aggregation, as well as change the secondary structure of amyloid fibrils [9–15]. Specifically, Hannestad and co-workers found that α-syn not only aggregated on the surfaces of lipid membranes, but strongly perturbed membrane integrity [16]. The Claessens group showed that α-syn–lipid interactions could be altered by the charge and the size of lipid vesicles [17–23]. Importantly, lipid-induced changes in the secondary structure of α-syn oligomers and fibrils

Abbreviations
α-Syn, alpha-synuclein; AFM, atomic force microscopy; AFM-IR, atomic force microscopy infrared spectroscopy; Cho, cholesterol; DMPS, 1,2-dimyristoyl-sn-glycero-3-phospho-L-serine; DOPC, 1,2-dioleoyl-sn-glycero3-phosphocholine; DOPS, 1,2-dioleoyl-sn-glycero-3-phospho-L-serine; DPPC, 1,2-dipalmitoyl-sn-glycero-3-phosphocholine; DMPC, 1,2-dimyristoyl-sn-glycero-3-phosphatidylcholine; FTIR, Fourier-transformed Infrared spectroscopy; LBs, Lewy bodies; LDH, lactate dehydrogenase; LUVs, large unilamellar vesicles; PBS, phosphate buffer saline; PD, Parkinson's disease; POPS, 1-palmitoyl-2-oleoyl-sn-glycero-3-phospho-L-serine; QCL, quantum-cascade laser; SM, sphingomyelin; $t_{1/2}$, half-time; ThT, thioflavin T; t_{lag}, lag-time; WT, wild-type.

uniquely alter their cytotoxicity [9,24]. These effects are determined by the chemical structure of lipids, as well as by the length and saturation of fatty acids (FAs) in the lipids [11,25,26].

DNA sequencing of patients with a family history of PD allowed for the identification of several mutations that were linked to the early-onset (A30P, E46K, and A53T) and late-onset (H50Q) forms of PD [27]. The Galvagnion group found that anionic 1,2-dimyristoyl-sn-glycero-3-phospho-L-serine (DMPS) accelerated the aggregation rate of WT α-syn, as well as A30P, and A53T α-syn mutants [12]. Our group showed that this effect could be altered by the length and saturation of FAs in PS [28]. Specifically, C14:0 PS (DMPS) caused significantly stronger acceleration of the WT α-syn compared to C18:0 (1,2-distearyl-sn-glycero-3-phospho-L-serine, DSPS) and PS with unsaturated FAs (1,2-dioleoyl-sn-glycero-3-phospho-L-serine (DOPS) and 1-palmitoyl-2-oleoyl-sn-glycero-3-phospho-L-serine (POPS) [28]. However, this relationship was not observed for A30P and A53T α-syn mutants. Furthermore, WT α-syn:DSPS fibrils exerted much weaker cytotoxic effects on rat dopaminergic neurons compared to WT α-syn. However, cytotoxicity of A30P:DSPS and A53T:DSPS fibrils were similar to A30P and A53T α-syn, respectively [28]. These results indicate that familial mutations in α-syn change protein–lipid interactions. Holman and co-workers recently reported that WT α-syn formed in the presence of 1,2-dipalmitoyl-sn-glycero-3- phosphocholine (DPPC), 1,2-dioleoyl-sn-glycero3-phosphocholine (DOPC), 30-bis[1,2-distearoylsn-glycero-3-phospho]-glycerol and 30-bis[1,2-dilinoleoyl-sn-glycero-3-phospho]-glycerol, as well as mixtures of these phospholipids, exert significantly higher cell toxicity compared to the protein aggregates formed in the lipid-free environment [29]. Furthermore, diet supplementation of these lipids to *C. elegans* altered their lifespan [29]. Recently, Matveyenka and co-workers found that cholesterol strongly accelerated the rate of α-syn aggregation [24]. Specifically, an increase in the concentration of cholesterol from 10% to 45% in large unilamellar vesicles (LUVs), composed of dipalmitoyl-sn-glycero-3-phosphatidylcholine (DPPC), increased the rate of WT α-syn aggregation [24]. However, the effect of cholesterol on the aggregation properties of α-syn mutants remains unclear.

In this study, we investigate the relationship between the cholesterol concentration and the rate of A30P, E46K, A53T, H50Q and WT α-Syn aggregation. We also determine the effect of sphingomyelin (SM) and 1,2-dimyristoyl-sn-glycero-3-phosphatidylcholine (DMPC) on the aggregation rate of these mutants. Using atomic force microscopy (AFM) and nano-Infrared spectroscopy, also known as atomic force microscopy Infrared (AFM-IR) spectroscopy, we examined the morphology and secondary structure of A30P, E46K, A53T, H50Q and WT α-Syn fibrils formed in the presence of LUVs composed of 10:90, 45:55, and 60:40 mol:mol ratios of cholesterol:DMPC that represent low, physiological and elevated concentrations of cholesterol in plasma membranes of neurons [30]. We also investigated the effect of LUVs composed of 10:90, 24:66, and 40:60 mol:mol ratios of SM:DMPC, which aim to model plasma membranes with low, normal, and high concentrations of SM [30]. Finally, cell assays were used to investigate the relationship between the secondary structure of A30P, E46K, A53T, H50Q and WT α-Syn fibrils and their toxicity to rat dopaminergic cells.

Results

Kinetic studies of protein aggregation in the presence of LUVs with different concentrations of DMPC, Cho and SM, as well as in the lipid-fee environment

In the lipid-free environment, WT α-syn aggregated with a well-defined lag-phase (t_{lag} = 12.48 ± 1.14 h) that was extended to (t_{lag} = 29.25 ± 3.334 h) in the presence of 100% DMPC LUVs, Fig. 1. With an increase in the concentration of Cho in the LUVs, t_{lag} gradually decreased from 22.61 ± 0.44 h (10:90 Cho:DMPC) to 12.81 ± 0.78 h (60:40 Cho:DMPC). Based on these results, we could conclude that Cho accelerated, while DMPC decelerated WT α-syn aggregation. Our results also indicate that LUVs, except 45:55 Cho:DMPC, did not have a significant effect on the rate of fibril formation ($t_{1/2}$), Fig. 1. Thus, DMPC and Cho:DMPC LUVs primarily interact with monomeric WT α-syn, rather than being involved in fibril elongation

Fig. 1. Lipids alter the rate of WT and A30P α-syn aggregation. Kinetic studies of WT and A30P α-syn aggregation in the presence of LUVs with different concentrations of 1,2-dimyristoyl-sn-glycero-3-phosphatidylcholine (DMPC), cholesterol (Cho) and sphingomyelin (SM). Thioflavin T plots (A, C, E, G) with corresponding bar graphs (B, D, F, H) of t_{lag} and $t_{1/2}$. Each curve shown in panels A, C, E and G is the average of three sample replicates (n = 3). The graphical data are presented as the mean ± SEM. According to one-way ANOVA, $^{**}P < 0.01$; $^{***}P < 0.001$. NS, nonsignificant differences.

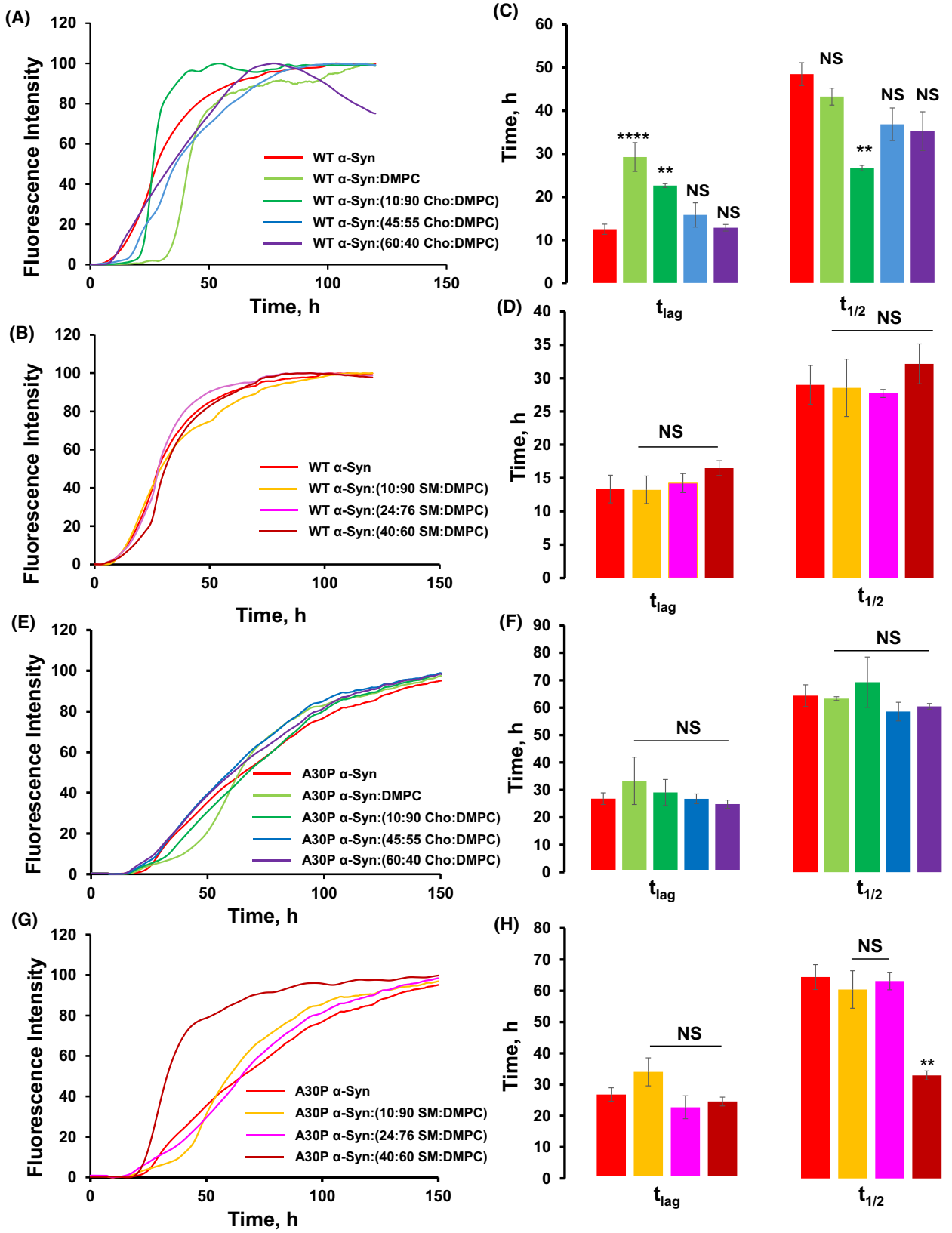

and secondary nucleation. ThT assay also revealed that, unlike Cho, SM did not have an effect on either t_{lag} or $t_{1/2}$ of WT α-syn aggregation.

Interestingly, A30P mutant of α-syn fully disabled protein–lipid interactions. This conclusion could be made based on ThT analyses of A30P α-syn interaction with DMPC, SM:DMPC, and Cho:DMPC LUVs. We also found that DMPC LUVs delayed the lag-phase of E46K α-syn (t_{lag} = 26.74 ± 0.85 h) that aggregated much faster (t_{lag} = 8.44 ± 0.25 h) compared to WT α-syn (t_{lag} = 12.48 ± 1.14 h), Fig. 2. Our results also showed that 60:40 Cho:DMPC LUVs accelerated (t_{lag} = 9.61 ± 0.21 h) the aggregation rate of E46K α-syn much stronger than 10:90 Cho:DMPC LUVs (t_{lag} = 11.24 ± 0.81 h). However, this effect was not as pronounced for 45:55 Cho:DMPC (t_{lag} = 19.92 ± 0.75 h). Thus, we can conclude that the E46K mutation significantly altered α-syn–Cho interactions. These conclusions are further supported by the analyses of $t_{1/2}$ of E46K α-syn aggregation. We also found that LUVs that contained 10% (t_{lag} = 17.43 ± 0.59 h), 24% (t_{lag} = 12.75 ± 0.71 h), and 40% (t_{lag} = 18.41 ± 0.95 h) of SM significantly delayed the lag-phase of E46K α-syn aggregation (t_{lag} = 8.44 ± 0.25 h), Fig. 2. Based on these results, we can conclude that E46K mutation in α-syn strongly altered protein–SM interactions.

ThT kinetics revealed that DMPC and Cho had similar effects on H50Q α-syn aggregation as for WT α-syn. Specifically, DMPC LUVs delayed the lag-phase of H50Q α-syn aggregation (t_{lag} = 4.31 ± 0.21 h), while this effect was mitigated by the presence of Cho in such LUVs. Specifically, 60:40 Cho:DMPC LUVs had the strongest acceleration effect on the lag-phase (t_{lag} = 2.01 ± 0.32 h) compared to 10:90 (t_{lag} = 2.71 ± 0.02 h) and 45:55 (t_{lag} = 3.00 ± 0.08 h) Cho:DMPC LUVs, Fig. 2. The same effect of Cho was observed on the rate ($t_{1/2}$) of protein aggregation. We found an increase in $t_{1/2}$ with an increase in the concentration of Cho in LUVs exposed to H50Q α-syn. We also found that H50Q α-syn exhibited similar interactions with SM as E46K α-syn, Fig. 2. Specifically, a delay in t_{lag} was observed in the presence of LUVs with 10%, 24% and 40% of SM t_{lag} = 4.41 ± 0.05 h, t_{lag} = 4.04 ± 0.08hand t_{lag} = 4.33 ± 0.01 h, respectively. Similar delay was observed in $t_{1/2}$ for 24:76 SM:DMPC and 40:60 SM:DMPC LUVs $t_{1/2}$ = 13.64 ± 0.05 h, $t_{1/2}$ = 12.84 ± 0.08hand $t_{1/2}$ = 12.83 ± 0.01 h, respectively. These results indicate that a H50Q mutation did not significantly alter protein–Cho interaction. However, this mutation had a strong impact on α-syn–SM interactions.

ThT assay showed that A53T α-syn (t_{lag} = 9.31 ± 0.24 h) aggregated slightly faster than WT α-syn (t_{lag} = 12.48 ± 1.14 h), Fig. 3. Similar to WT α-syn, DMPC LUVs delayed the lag-phase of A53T α-syn aggregation (t_{lag} = 12.35 ± 0.21 h), while low (t_{lag} = 7.58 ± 0.50 h) and medium (t_{lag} = 7.684 ± 0.32 h) concentrations of Cho in LUVs shortened the lag-phase of A53T α-syn aggregation. However, high concentrations of Cho, on the other hand, strongly delayed the lag-phase (t_{lag} = 12.81 ± 0.81 h) of A53T α-syn aggregation, Fig. 3. These results indicate that A53T mutation altered protein–Cho interactions. These conclusions are further supported by the kinetic analysis of A53T α-syn aggregation in the presence of SM LUVs. Specifically, we found that an increase in the concentration of SM in LUVs resulted in the acceleration of A53T α-syn aggregation, which was not observed for WT α-syn. Based on these results, we can conclude that mutations in α-syn drastically alter protein–lipid interactions, which results in the increase or decrease of the lag-phase of the α-syn aggregation and the rate of fibril formation.

Morphological characterisation of protein aggregates formed in the presence of LUVs with different concentrations of DMPC, Cho and SM, as well as in the lipid-free environment

Microscopic analysis of amyloid samples revealed that in the lipid-free environment, WT α-syn formed long fibrillar species with heights ranging from 9 to 18 nm, Figs 4–6 and Table S1. Significantly shorter and thinner fibrils were observed in WT α-syn:DMPC, as well as in WT α-syn:(10:90 SM:DMPC) and WT α-syn:(24:76 SM:DMPC). However, in the presence of 60:40 SM:DMPC, WT α-syn developed long fibrillar structures that were not observed at low concentrations of SM in LUVs, Figs 4–6 and Table S1. Thus, we can conclude that DMPC and high concentrations of SM substantially alter the morphology of WT α-syn fibrils. We also found that the presence of

Fig. 2. Lipids alter the rate of E46K and H50Q α-syn aggregation. Kinetic studies of E46K and H50Q α-syn aggregation in the presence of LUVs with different concentrations of 1,2-dimyristoyl-sn-glycero-3-phosphatidylcholine (DMPC), cholesterol (Cho) and sphingomyelin (SM). Thioflavin T plots (A, C, E, G) with corresponding bar graphs (B, D, F, H) of t_{lag} and $t_{1/2}$. Each curve shown in panels A, C, E, G is the average of three sample replicates (n = 3). The graphical data are presented as the mean ± SEM. According to one-way ANOVA, *P < 0.05; **P < 0.01; ****P < 0.001; ****P < 0.0001. NS, nonsignificant differences.

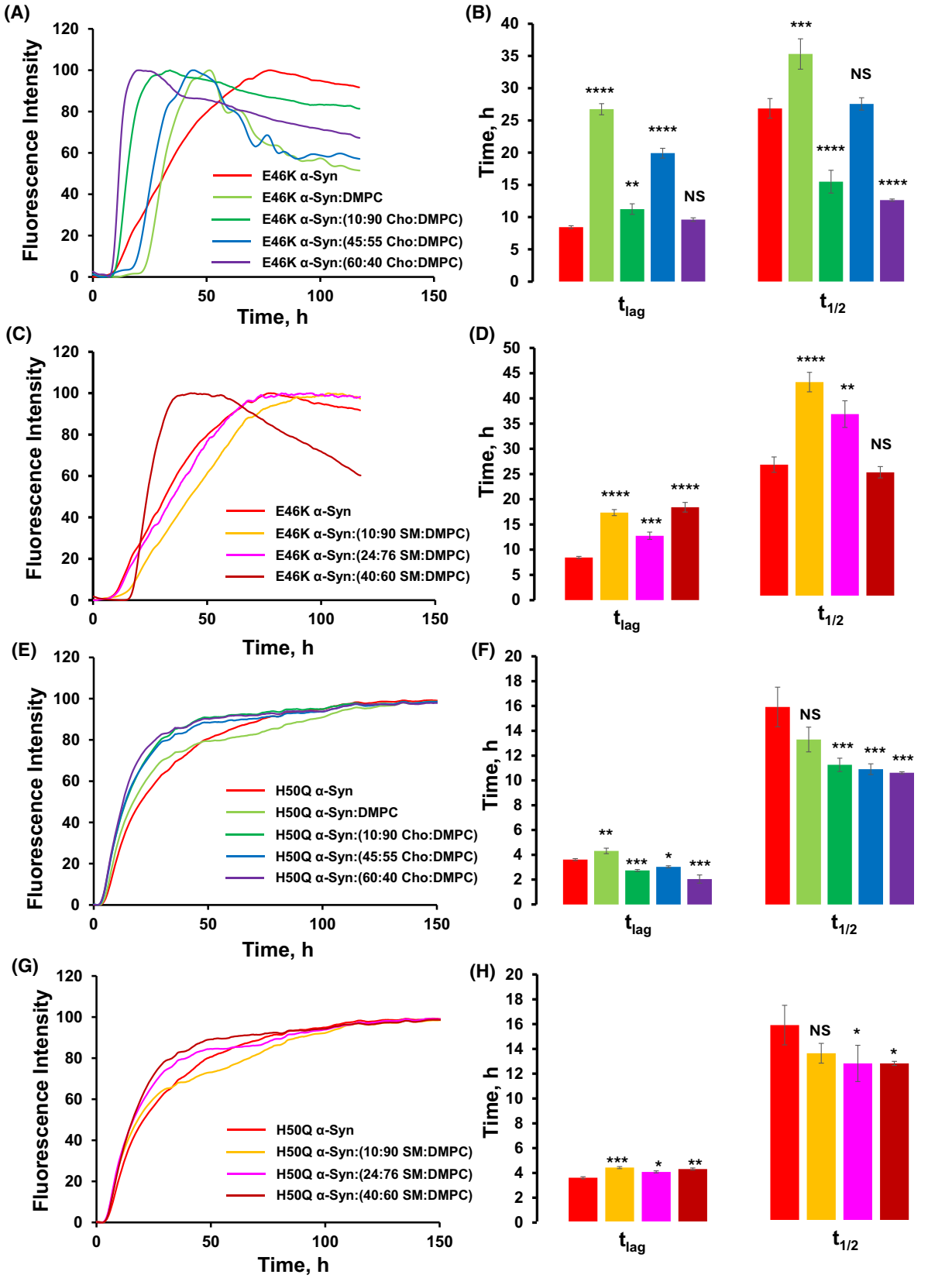

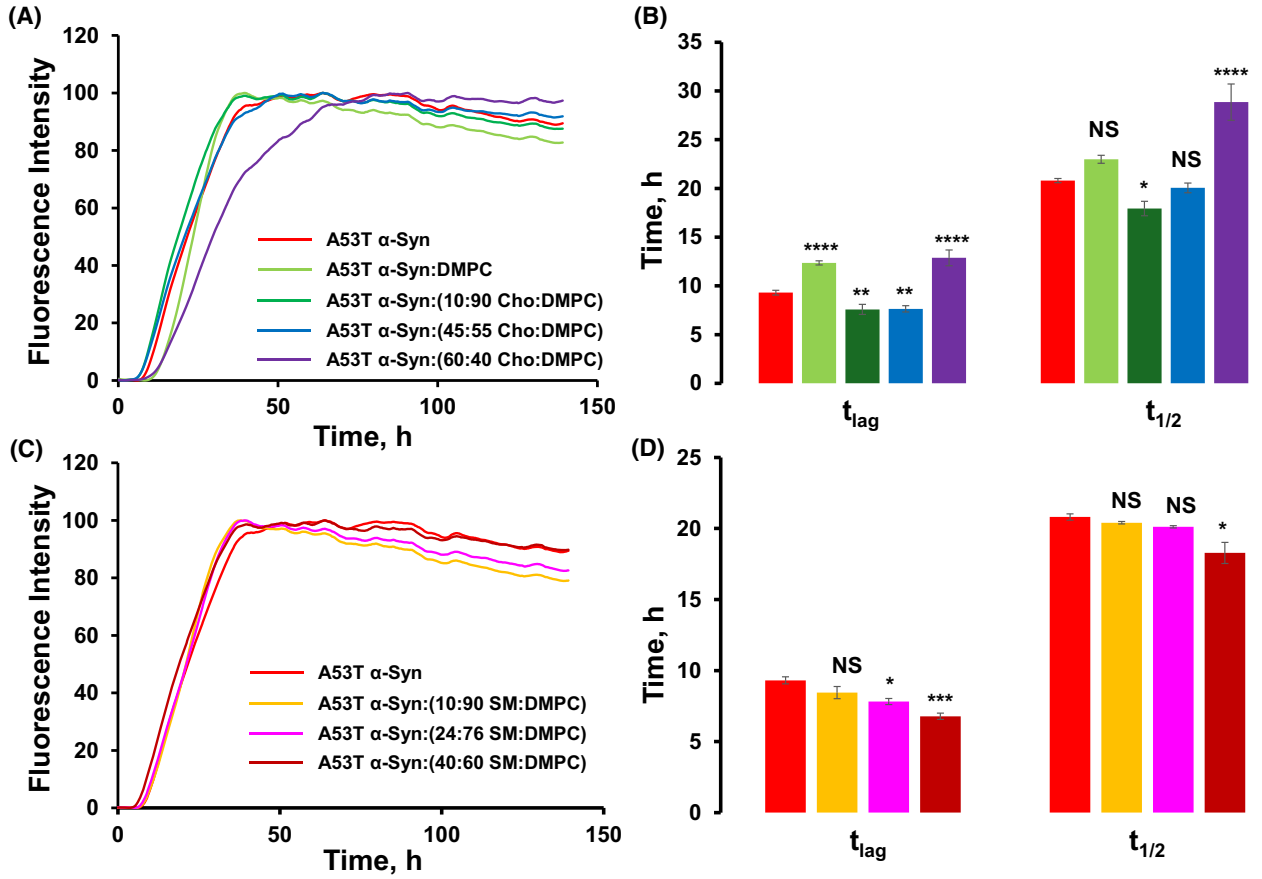

Fig. 3. Lipids alter the rate of A63T α-syn aggregation. Kinetic studies of A53T α-syn aggregation in the presence of LUVs with different concentrations of 1,2-dimyristoyl-sn-glycero-3-phosphatidylcholine (DMPC), cholesterol (Cho) and sphingomyelin (SM). Thioflavin T plots (A and C) with corresponding bar graphs (B and D) of t_{lag} and $t_{1/2}$. Each curve shown in panels A, C, E and G is the average of three sample replicates ($n = 3$). The graphical data are presented as the mean ± SEM. According to one-way ANOVA, $^{*}P < 0.05$; $^{**}P < 0.01$; $^{***}P < 0.001$; $^{****}P < 0.0001$. NS, nonsignificant differences.

Cho in DMPC LUVs did not substantially alter the morphology of WT α-syn aggregates. Specifically, in all samples, we observed fibrillar structures with similar heights (6–18 nm) to those formed in the lipid-free environment, Figs 4–6 and Table S1. These results are in good agreement with experimental findings that were previously reported by our group for DPPC:Cho LUVs [24]. Thus, we can conclude that Cho does not significantly change the morphology of WT α-syn aggregates.

No substantial morphological changes were also evident in A30P α-syn:lipid samples compared to the fibrils observed in A30P α-syn. Specifically, in all samples formed by A30P α-syn, morphologically similar fibrils with 6–18 nm in height were observed. Our results show that in the lipid-free environment, E46K α-syn formed only short fibrillar species with 6–12 nm in height, Figs 4–6 and Table S1. Morphologically similar species, however, with larger lengths, were observed in E46K α-syn:DMPC and E46K α-syn:(Cho:DMPC) samples, Figs 4–6. These results indicate that both DMPC and Cho did not significantly alter the morphology of E46K α-syn fibrils. At the same time, the presence of SM in LUVs resulted in the formation of thick and long protein aggregates. Based on these results, we could conclude that SM drastically altered the morphology of E46K α-syn fibrils.

In the lipid-free environment, H50Q α-syn aggregated, forming long fibrils with 6–18 nm in height. Morphologically similar fibrils were observed in H50Q α-syn:DMPC, H50Q α-syn:(Cho:DMPC), and H50Q α-syn:(SM:DMPC) samples, Figs 4–6 and Table S1. These results indicate that neither DMPC, Cho or SM substantially alter the morphology of H50Q α-syn aggregates. The same conclusions could be made about A53T α-syn aggregates. In the absence of LUVs, A53T α-syn formed long fibrils that were 6–15 nm in height,

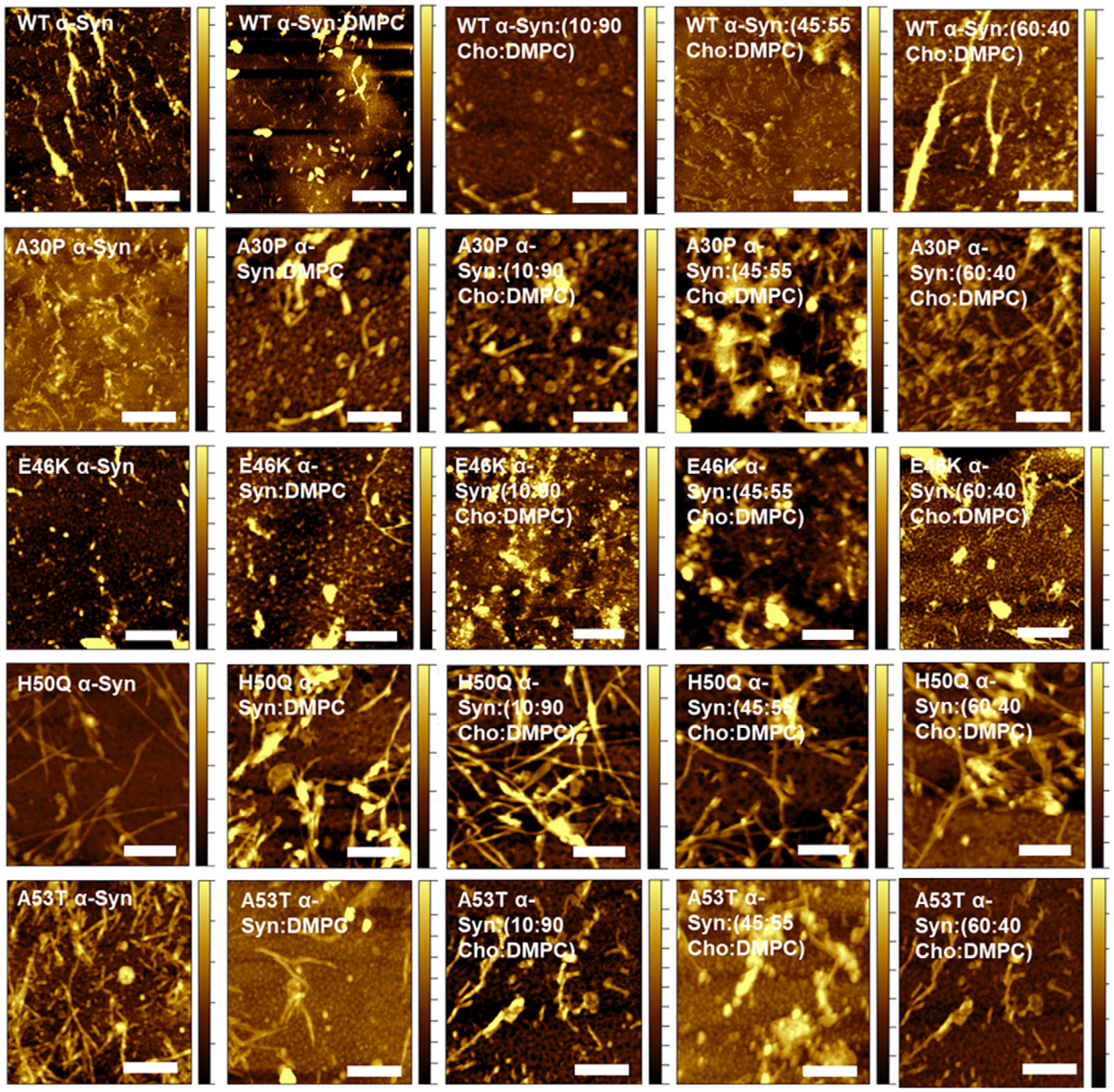

Fig. 4. Lipids alter the morphology α-syn aggregates. Atomic force microscopy images of WT, A30P, E46K, H50Q and A53T α-syn aggregates formed in the presence of LUVs with different concentrations of 1,2-dimyristoyl-sn-glycero-3-phosphatidylcholine (DMPC) and cholesterol (Cho), as well as in the lipid-free environment. Scale bars are 500 nm. Spherical aggregates are oligomers; prolonged rope-like aggregates are fibrils. Height values of Z axes are summarised in Table S1.

Figs 4–6 and Table S1. Morphologically similar fibrils were found in A53T α-syn:DMPC, A53T α-syn:(Cho:DMPC), and A53T α-syn:(SM:DMPC) samples. Thus, these findings indicated that the presence of LUVs with DMPC, SM and Cho had no effect on the morphology of A53T α-syn fibrils.

Finally, AFM revealed the presence of LUVs (H50Q α-syn:(SM:DMPC), A53T α-syn:(SM:DMPC), and A30P α-syn:DMPC) and lipid droplets (A30P α-syn:(10:90 SM:DMPC) and A30P α-syn:(45:55 SM:DMPC)) in some of the analysed samples. Although intact LUVs were typically observed by themselves, lipid droplets were surrounded by fibrils, which further supports our own results and experimental findings reported by other groups that lipids facilitated the aggregation of α-syn [11–13,29].

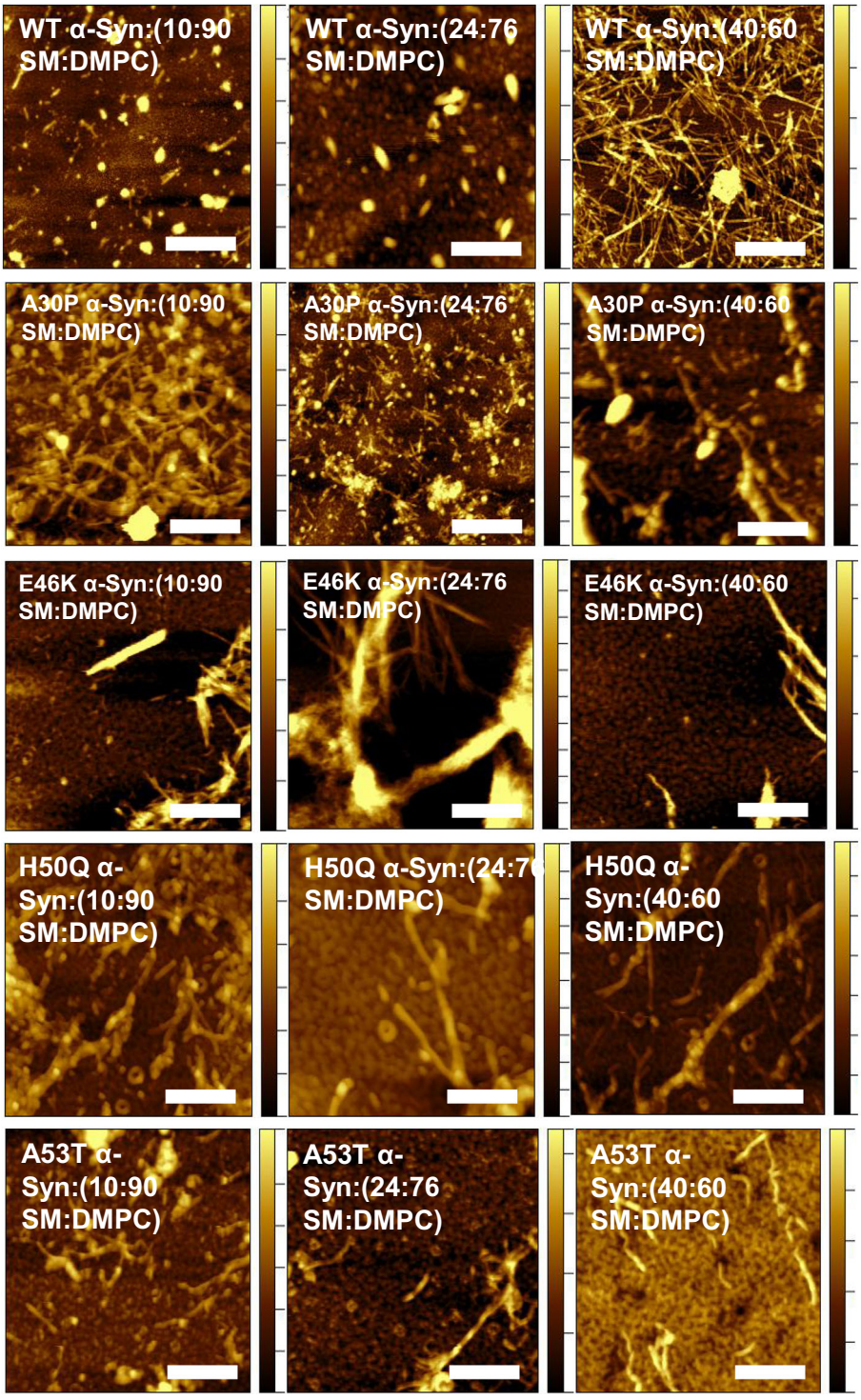

Fig. 5. Lipids alter the morphology of α-syn aggregates. Atomic force microscopy images of WT, A30P, E46K, H50Q and A53T α-syn aggregates formed in the presence of LUVs with different concentrations of 1,2-dimyristoyl-sn-glycero-3-phosphatidylcholine (DMPC) and sphingomyelin (SM). Scale bars are 500 nm. Spherical aggregates are oligomers; prolonged rope-like aggregates are fibrils. Height values of Z axes are summarised in Table S1.

Structural characterisation of protein aggregates formed in the presence of LUVs with different concentrations of DMPC, Cho and SM, as well as in the lipid-free environment

We used CD and FTIR to perform spectroscopic analysis of protein samples after 150 h of aggregation at 37 °C and 510 rpm agitation. CD spectra acquired from all samples had a minimum around 220 nm, indicating the presence of β-sheet, Figs 7–9. The same conclusion could be drawn by the analysis of amide I band in the acquired FTIR spectra. In all collected spectra, amide I band was centred around 1630–1636 cm^{-1}, which indicates the predominance of parallel β-sheet, Figs 7–9. We hypothesised that small variability in the peak position of amide I band could be caused by the presence of unaggregated protein in all samples. To overcome this issue, we utilised nano-IR spectroscopy that allows for positioning the scanning probe directly at the aggregate of interest present in the sample and to acquire IR spectra [31–35].

AFM-IR revealed that WT α-syn fibrils grown in the lipid-free environment had a nearly equal (~30%) amount of parallel, anti-parallel β-sheet, and a random coil secondary structure. We also found that the presence of DMPC drastically lowered the amount of parallel β-sheet in WT α-syn fibrils, Fig. 10. However, the presence of Cho in the LUVs did not result in structural differences in WT α-syn fibrils formed under the experimental conditions described above. We also found that the presence of LUVs with 10:90 SM:DMPC ratio resulted in the formation of fibrils with a highly rich parallel β-sheet. At the same time, WT α-syn fibrils formed in the presence of LUVs with 24:76 SM:DMPC and 60:40 SM:DMPC had the same secondary structure as WT α-syn fibrils grown in the lipid-free environment, Fig. 10.

We also found that a high concentration of Cho and SM in LUVs resulted in an increase in the amount of parallel β-sheet in A30P α-syn fibrils, Fig. 11. However, the presence of other LUVs did not alter the secondary structure of A30P α-syn fibrils. The same conclusion could be made about E46K α-syn aggregates. We observed an increase in the amount of parallel β-sheet only in the protein aggregates that were grown in the presence of 60:40 Cho:DMPC LUVs, Fig. 12.

In H50Q, α-syn fibrils formed in the presence of DMPC, and we observed a decrease in the amount of parallel β-sheet. The same decrease was observed in the presence of 45:55 Cho:DMPC and 60:40 Cho:DMPC LUVs, as well as in the presence of all SM LUVs, Fig. 13. These results indicate that the secondary structure of H50Q α-syn fibrils is strongly affected by Cho and SM. Finally, we found that A53T α-syn fibrils formed in the presence of DMPC and Cho:DMPC LUVs had the same secondary structure as A53T α-syn fibrils formed in the lipid-free environment, Fig. 14. Only protein aggregates that were grown in the presence of 24:76 SM:DMPC had a significantly lower amount of parallel β-sheet.

Based on these results, we can conclude that DMPC, SM and Cho caused substantial changes in the secondary structure of WT, A30P, E46K, H50Q, and A53T α-syn fibrils at some concentrations. This concentration effect was directly dependent on the type of lipid and mutation in α-syn. Additional studies are required to fully understand the relationship between the chemical structure of lipids, its concentration and the effect exerted on each particular α-syn mutant.

Cytotoxicity of protein aggregates formed in the presence of LUVs with different concentrations of DMPC, Cho and SM, as well as in the lipid-free environment

To examine cytotoxicity of α-syn fibrils formed in the presence of LUVs with different concentrations of DMPC, Cho and SM, as well as in the lipid-free environment, rat dopaminergic neurons were used. Using LDH assay, we investigated viability of these cells after 24 h exposure to the fibrils. Our results indicated that WT α-syn fibrils exerted significant toxicity to rat dopaminergic neurons, Fig. 15. We found that the presence of 45:55 Cho:DMPC and 60:30 Cho:DMPC LUVs resulted in the formation of more toxic fibrils compared to WT α-syn aggregates formed in the lipid-free environment. These results are in good agreement with our previous findings [36]. At the same time, the presence of LUVs with SM did not alter the cytotoxicity of WT α-syn fibrils.

Interestingly, LUVs did not alter the cytotoxicity of A30P α-syn fibrils. At the same time, E46K α-Syn fibrils formed in the presence of 60:40 Cho:DMPC were found to be significantly more toxic, while those formed in the presence of 10:90 SM:DMPC LUVs were less toxic to the neurons, Fig. 15. LDH assay also revealed that H50Q and A53T α-syn fibrils formed in the presence of LUVs composed of DMPC, SM and Cho were less toxic compared to H50Q and A53T α-syn fibrils formed in the lipid-free environment, respectively. Thus, we can conclude that for all mutants, except A30P, α-syn—as well as for WT α-syn—DMPC, Cho and SM alter cytotoxicity of amyloid fibrils.

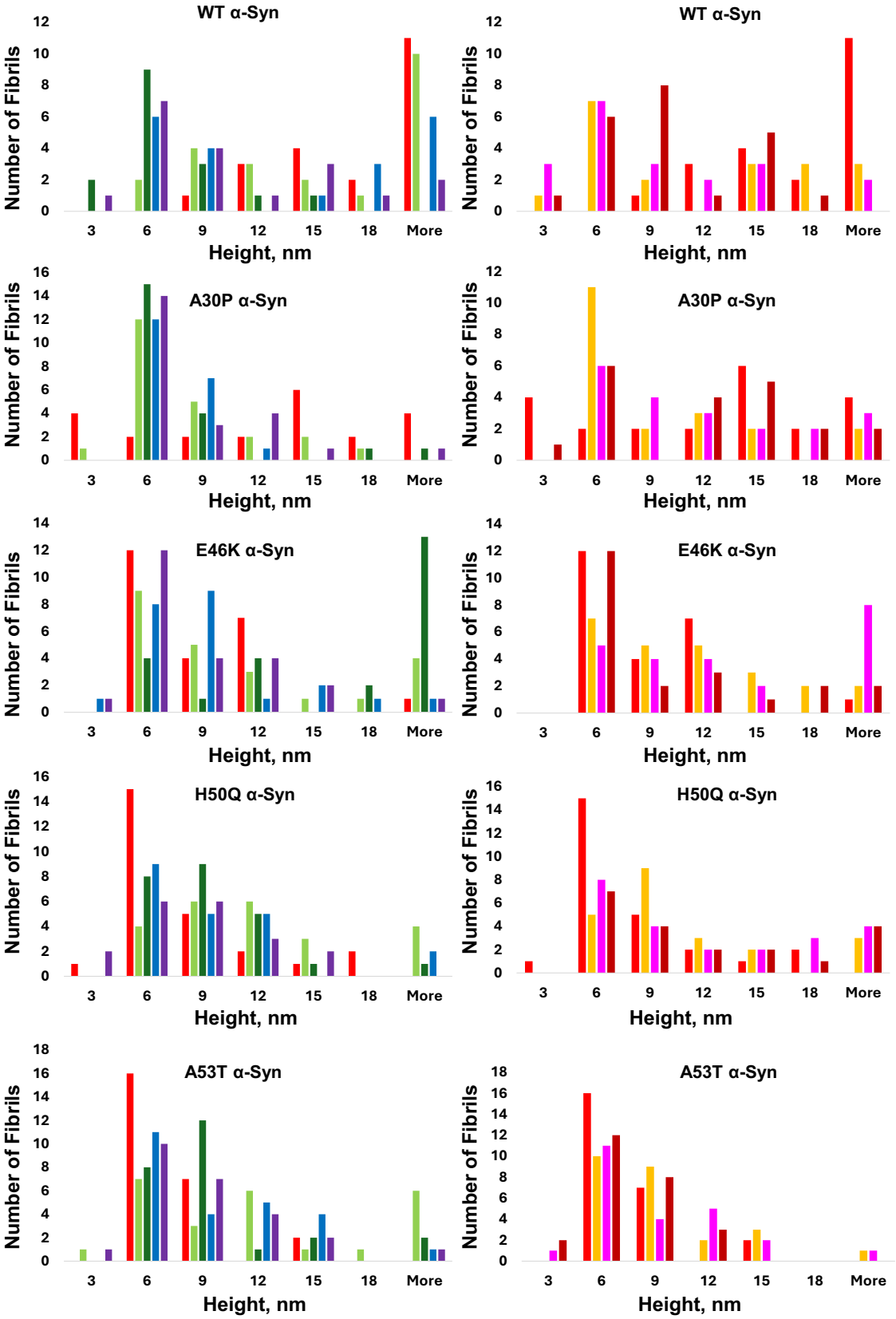

Fig. 6. Lipids alter the morphology of α-syn aggregates. Height histograms of WT, A30P, E46K, H50Q and A53T α-syn aggregates formed in the presence of LUVs with different concentrations of 1,2-dimyristoyl-sn-glycero-3-phosphatidylcholine (DMPC), cholesterol (Cho) and sphingomyelin (SM), as well as in the lipid-free environment. Lipid-free conditions are in red; DMPC in light green, (10:90 Cho:DMPC) in green, (45:55 Cho:DMPC) in blue, (60:40 Cho:DMPC) in purple, (10:90 SM:DMPC) in yellow, (24:76 SM:DMPC) in pink, and (40:60 SM:DMPC) in maroon. For each height profile, 10–20 individual aggregates were analysed.

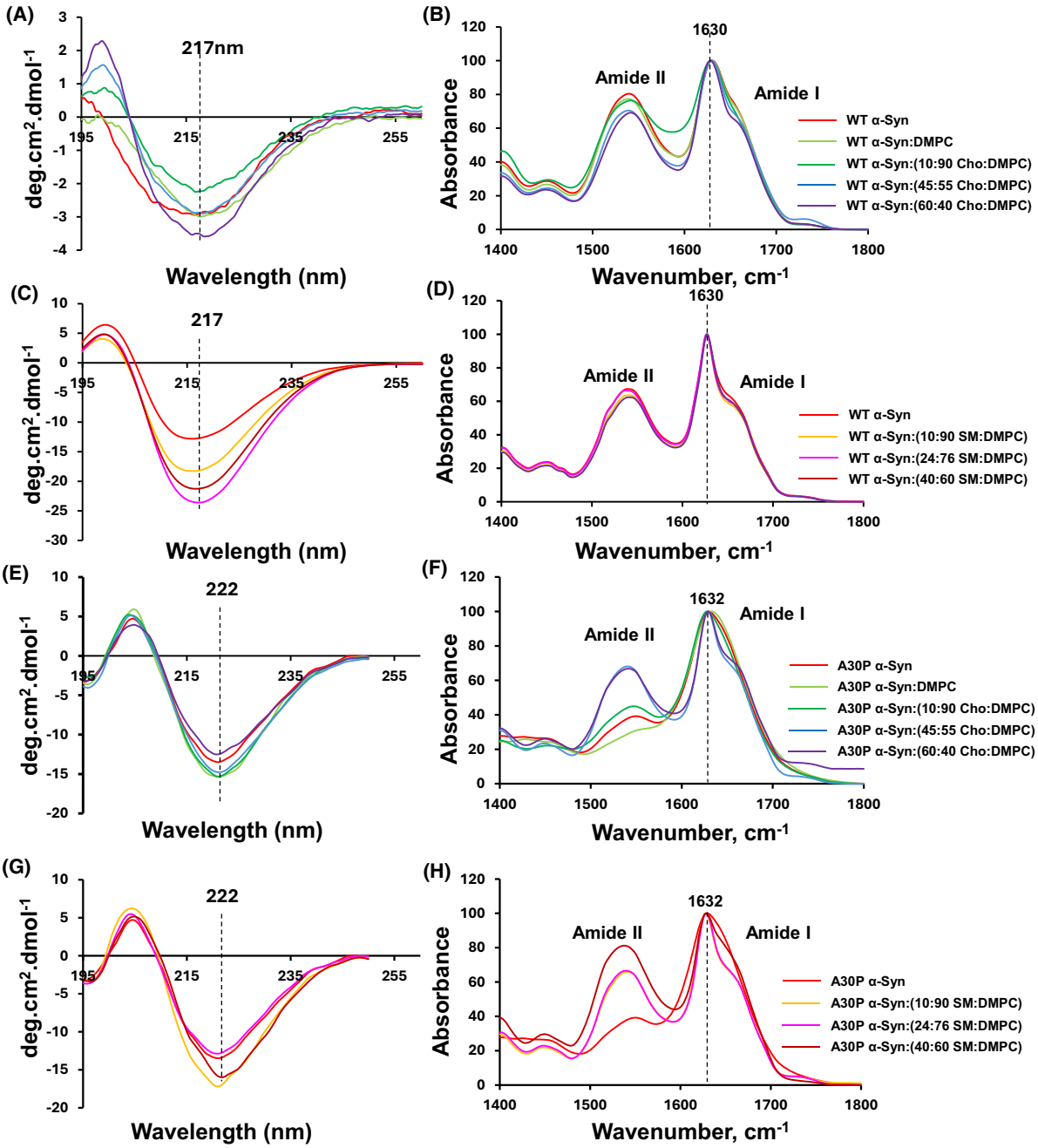

Fig. 7. Influence of lipids on the secondary structure of α-syn aggregates. CD (A, C, E, G) and normalised FTIR (B, D, F, H) spectra acquired from WT and A30P α-syn aggregation in the presence of LUVs with different concentrations of 1,2-dimyristoyl-sn-glycero-3-phosphatidylcholine (DMPC), cholesterol (Cho) and sphingomyelin (SM). Amide I and II bands originate from the vibration of amide bonds in proteins. FTIR spectra are normalised on amide I band. For each spectrum, three individual measurements were made.

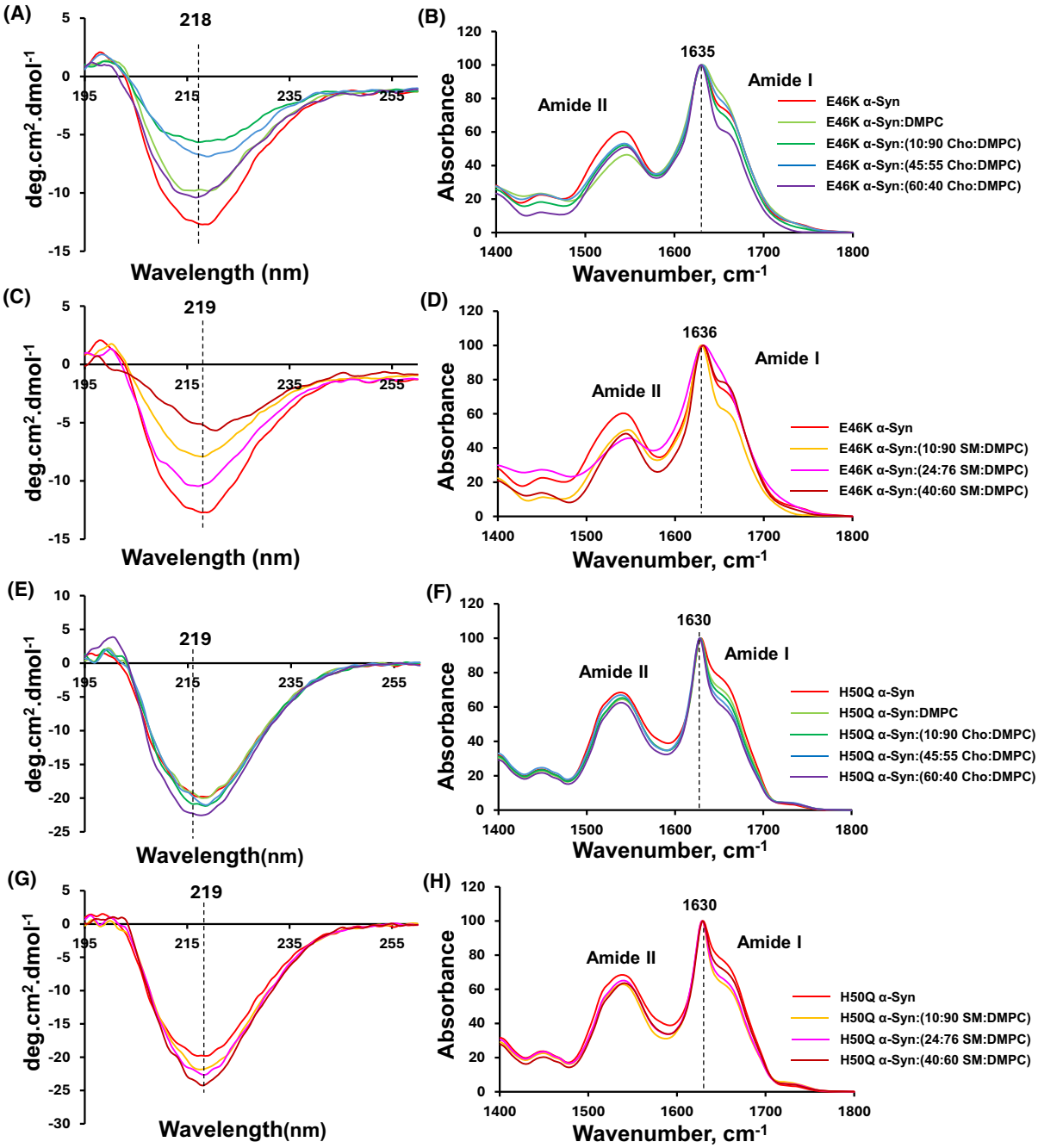

Fig. 8. Influence of lipids on the secondary structure of α-syn aggregates. Circular dichroism (A, C, E, G) and normalised Fourier-transformed Infrared (FTIR) (B, D, F, H) spectra acquired from E46K and H50Q α-syn aggregation in the presence of LUVs with different concentrations of 1,2-dimyristoyl-sn-glycero-3-phosphatidylcholine (DMPC), cholesterol (Cho) and sphingomyelin (SM). Amide I and II bands originate from the vibration of amide bonds in proteins. FTIR spectra are normalised on amide I band. For each spectrum, three individual measurements were made.

Discussion

The onset and progression of PD are linked to the abrupt aggregation of α-syn in the midbrain, thalamus and hypothalamus. This small cytosolic protein is mainly located in synaptic terminals [37]. Although the physiologic function of α-syn is not fully

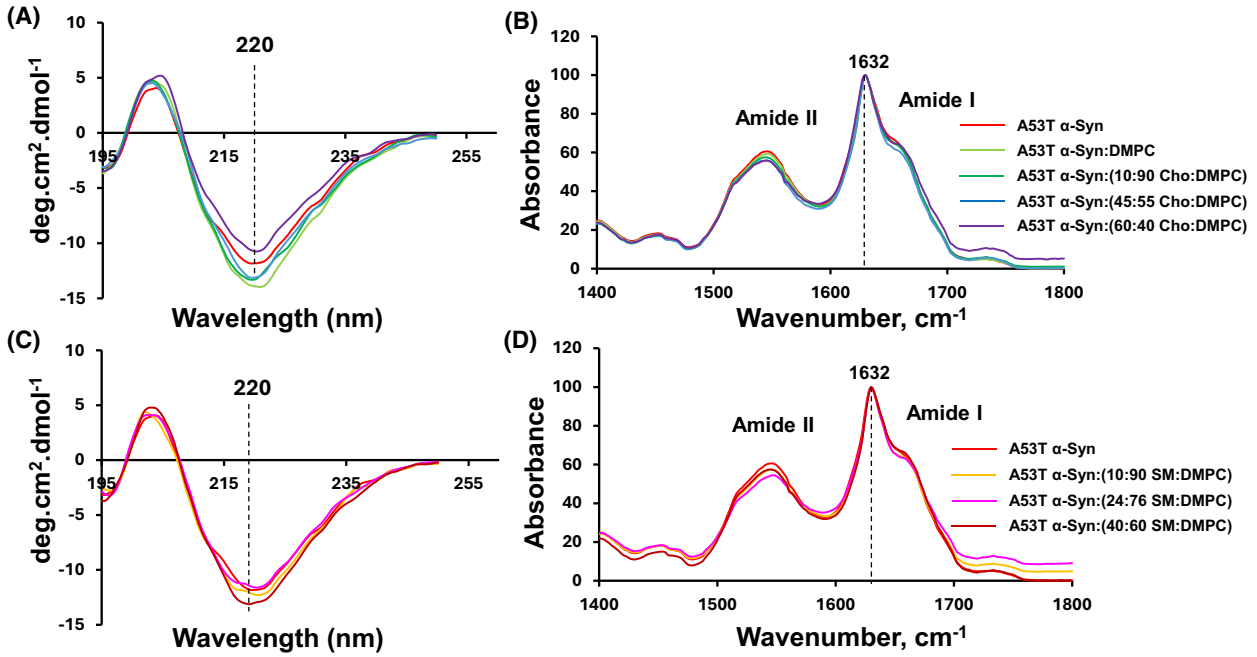

Fig. 9. Influence of lipids on the secondary structure of α-syn aggregates. Circular dichroism (A and C) and normalised Fourier-transformed Infrared (FTIR) (B and D) spectra acquired from A53T α-syn aggregation in the presence of LUVs with different concentrations of 1,2-dimyristoyl-sn-glycero-3-phosphatidylcholine (DMPC), cholesterol (Cho) and sphingomyelin (SM). Amide I and II bands originate from the vibration of amide bonds in proteins. FTIR spectra are normalised on amide I band. For each spectrum, three individual measurements were made.

understood [38–40], there is a growing body of evidence indicating the important role of α-syn in control of the neurotransmitter release in synaptic clefts, synaptic plasticity, and inflammatory response [10,41]. Intrinsically disordered, α-syn folds into an α-helical structure in the presence of lipid membranes [12,42]. This and other evidence indicates the importance of lipid bilayers for protein stability. Consequently, changes in the composition of lipid membranes could trigger protein aggregation. NMR and fluorescence spectroscopy demonstrated that in such cases, α-syn binds lipids via strong electrostatic interactions that take place between lysine and glutamic acid residues on the N-terminus (1–60 aa) of α-Syn and lipid headgroups [43]. α-Syn–lipid complexes are also stabilised by hydrophobic interactions that are established between fatty acids of lipids and the central domain (61–95 aa) of α-Syn [44,45]. Furthermore, such α-syn–lipid complexes irreversibly change the catalytic reactivity of cytoplasmic enzymes and lysosomal lipases, which results in PD-specific alterations of lipids in both the brain and plasma [46].

In our previous study, we examined the effect of PS with different length and saturation of FAs on the aggregation properties of WT α-syn, as well as on A30P and A53T α-syn mutants [28]. Our results showed that A30P and A53T mutations significantly altered the response of α-syn to PS LUVs compared to WT protein. We observed significant differences in the rate of protein aggregation, secondary structure of A30P α-syn:PS and α-syn:A53T fibrils, as well as the cytotoxicity that such protein aggregates exerted on rat dopaminergic neurons. However, it was unclear whether such effects are unique to PS or if they are common among a large group of lipids.

In the current study, we found that change in the aggregation properties of E46K, A53T, H50Q, and WT α-syn induced by DMPC, SM and Cho change are concentration-dependent. Similar concentration-dependent changes were observed in the toxicity that such protein aggregates exert on rat dopaminergic cells. We also found that A30P mutation has reduced membrane affinity α-syn–lipid interactions. As a result, no changes in the aggregation rate of A30P α-Syn were observed at different concentrations of DMPC, Cho and SM. This conclusion is further supported by lipid-independent cytotoxicity of A30P α-syn fibrils that were not observed for other mutants and WT α-syn. It is important to note that our results are in good agreement with those reported by other researcher groups [47–49].

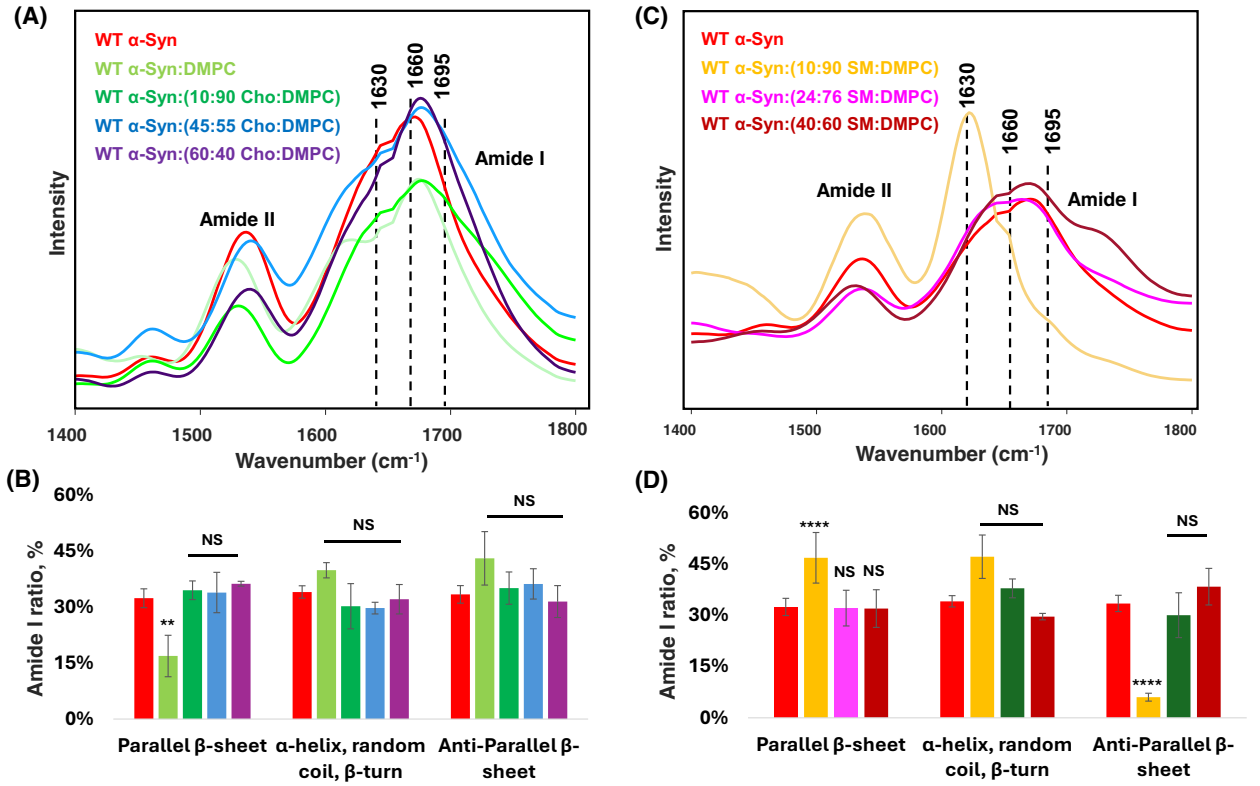

Fig. 10. Influence of lipids on the secondary structure of α-syn aggregates. Atomic force microscopy Infrared spectra (A and C) and histograms (B and D) showing the amount of parallel β-sheet, α-helix, random coil, and β-turn, as well as antiparallel β-sheet in the secondary structure of WT α-syn aggregates-grown presence of LUVs with different concentrations of 1,2-dimyristoyl-sn-glycero-3-phosphatidylcholine (DMPC), cholesterol (Cho) and sphingomyelin (SM), as well as in the lipid-free environment. Lipid-free conditions are in red; DMPC in light green, (10:90 Cho:DMPC) in green, (45:55 Cho:DMPC) in blue, (60:40 Cho:DMPC) in purple, (10:90 SM:DMPC) in yellow, (24:76 SM:DMPC) in pink, and (40:60 SM:DMPC) in maroon. Each curve shown in panels A–C is the average of three sample replicates ($n = 3$). The graphical data are presented as the mean ± SEM. According to one-way ANOVA followed by Tukey's HSD test $^{**}P < 0.01$, $^{****}P < 0.0001$. NS shows the absence of statistically significant differences.

In our previous study, we used cite-specific mutagenesis to identify charged lysines present in the N terminus of α-syn that determine protein–lipid interactions [25]. That work showed that there is more than one lysine that is responsible for such interactions, as well as revealing possible contributions of hydrophobic forces in the interactions between α-syn and lipids. The observed effect of A30P mutation in the N terminus of α-syn on DMPC, SM and Cho observed in the current study supported our hypothesis that not only electrostatic but also hydrophobic forces play a very important role in the interactions between α-syn and lipids. We additionally found that DMPC and the larger analogue of this peptide, dipalmitoylphosphatidylcholine (DPPC, C16:0) exerted similar effects on α-syn aggregation. Specifically, in our previous study, we showed that α-syn:DPPC fibrils had lower cytotoxicity compared to α-syn fibrils formed in the lipid-free environment [24]. Our current findings indicate that α-syn:DMPC fibrils also had lower cytotoxicity compared to α-syn fibrils formed in the absence of lipids. These results indicate that the length of FAs in the PC plays a less important role in α-syn–lipid interactions compared to the amino acid sequence of the protein N terminus.

It should be noted that the effect of DMPC, SM and Cho on the protein aggregation and cytotoxicity of amyloid aggregates directly depends on protein amino acid composition. In our previous study, we demonstrated that Cho accelerated the aggregation of transthyretin [30]. Furthermore, this effect directly depended on the concentration of Cho in LUVs. At the same time, SM and DMPC decelerated transthyretin aggregation. However, cytotoxicity of such Cho, SM and DMPC:transthyretin fibrils was lower compared to transthyretin aggregates formed in the lipid-free environment [30]. We also showed that DMPC and Cho decelerated the aggregation rate of Tau

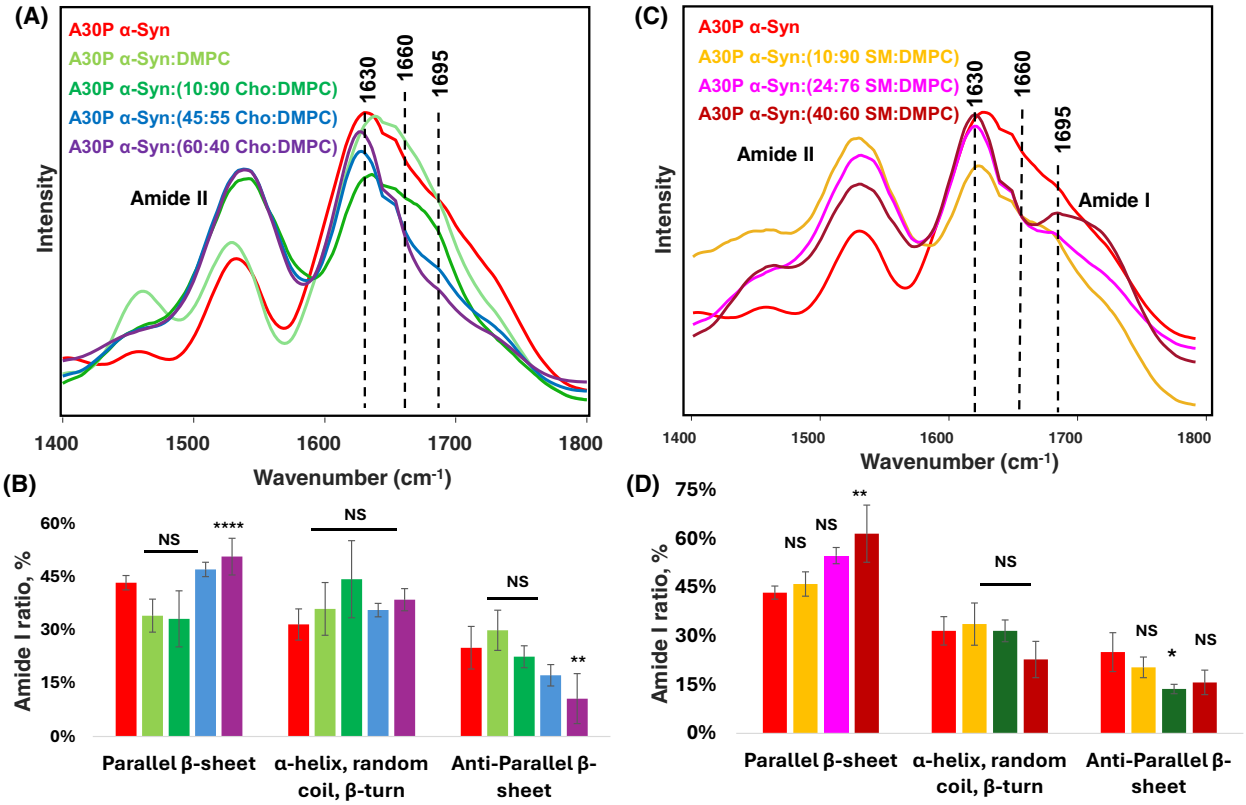

Fig. 11. Influence of lipids on the secondary structure of α-syn aggregates. Atomic force microscopy Infrared spectra (A and C) and histograms (B and D) showing the amount of parallel β-sheet, α-helix, random coil, and β-turn, as well as antiparallel β-sheet in the secondary structure of A30P α-syn aggregates-grown presence of LUVs with different concentrations of 1,2-dimyristoyl-sn-glycero-3-phosphatidylcholine (DMPC), cholesterol (Cho) and sphingomyelin (SM), as well as in the lipid-free environment. Lipid-free conditions are in red; DMPC in light green, (10:90 Cho:DMPC) in green, (45:55 Cho:DMPC) in blue, (60:40 Cho:DMPC) in purple, (10:90 SM:DMPC) in yellow, (24:76 SM:DMPC) in pink, and (40:60 SM:DMPC) in maroon. Each curve shown in panels A–C is the average of three sample replicates ($n = 3$). The graphical data are presented as the mean ± SEM. According to one-way ANOVA followed by Tukey's HSD test, $^{*}P < 0.05$, $^{**}P < 0.01$, **** < 0.0001. NS shows the absence of statistically significant differences.

isoforms with 0 (0N4R), 1 (1N4R) and 2 (2N4R) N repeats [50,51]. However, for all isoforms except 2N4R, cytotoxicity of such protein-lipid aggregates was higher than the cytotoxicity of 0N4R and 1N4R fibrils [51]. These results further support our conclusion that protein–lipid interactions directly depend on the amino acid sequence of amyloidogenic protein.

Conclusions

Our results showed that familial mutations in α-syn uniquely alter protein–lipid interactions. In some cases (A30P), mutations reduce protein–lipid interactions, while in others (E46K, H50Q, and A53T) proteins respond differently to the same lipid. This response includes but is not limited to the rate of protein aggregation, morphology and secondary structure of amyloid fibrils. These results highlight a complex nature of protein–lipid interactions that are taking place between N terminus of α-syn, polar heads and aliphatic tails of lipid FAs. These results also indicate that it is not only electrostatic interactions that play a very important role in protein–lipid interactions between charged lysines in the N terminus and polar heads of lipids [25], but also hydrophobic forces between non-polar amino acids, such as alanine. We additionally found that familial mutations uniquely attenuate cytotoxicity of α-syn fibrils. A30P mutation results in the formation of equally cytotoxic fibrils under different concentrations of DMPC, SM and Cho, while other mutations E46K, H50Q and A53T make amyloid fibrils more or less toxic with the particular lipid mixture. These results indicate that changes in lipid profiles of cell membranes could have a strong effect on the onset and progression of PD in individuals with familial mutations.

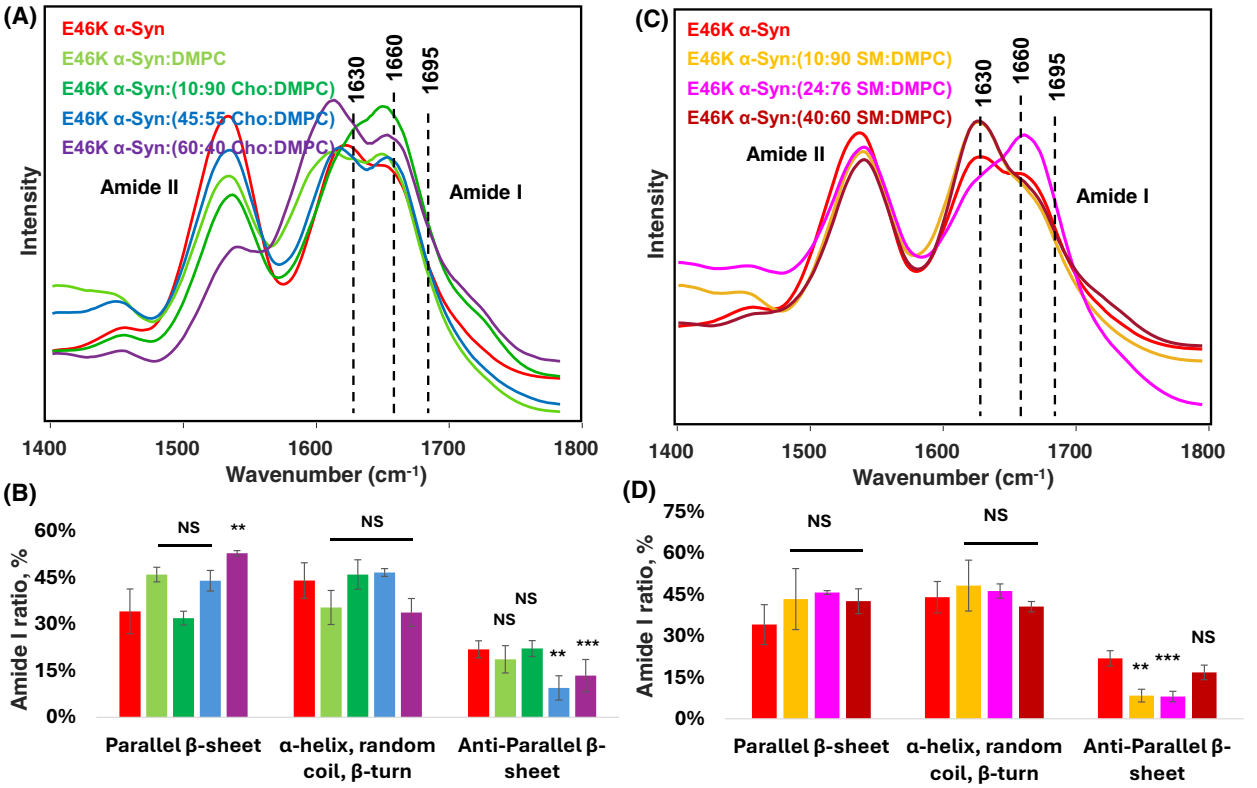

Fig. 12. Influence of lipids on the secondary structure of α-syn aggregates. Atomic force microscopy Infrared spectra (A and C) and histograms (B and D) showing the amount of parallel β-sheet, α-helix, random coil, and β-turn, as well as antiparallel β-sheet in the secondary structure of E46K α-syn aggregates-grown presence of LUVs with different concentrations of 1,2-dimyristoyl-sn-glycero-3-phosphatidylcholine (DMPC), cholesterol (Cho) and sphingomyelin (SM), as well as in the lipid-free environment. Lipid-free conditions are in red; DMPC in light green, (10:90 Cho:DMPC) in green, (45:55 Cho:DMPC) in blue, (60:40 Cho:DMPC) in purple, (10:90 SM:DMPC) in yellow, (24:76 SM:DMPC) in pink, and (40:60 SM:DMPC) in maroon. Each curve shown in panels A–C is the average of three sample replicates ($n = 3$). The graphical data are presented as the mean ± SEM. According to one-way ANOVA followed by Tukey's HSD test, $^{**}P < 0.01$, $^{***}P < 0.001$. NS shows the absence of statistically significant differences.

Materials and methods

Materials

(DMPC 14:0) 1,2-dimyristoyl-sn-glycero-3-phosphocholine, cholesterol and sphingomyelin (Brain, Porcine) were purchased from Avanti (Alabaster, AL, USA); IPTG was purchased from SIGMA USA.

Cloning and site direct mutagenesis of the α-synuclein, A30P, A53T, E46K and H50Q

plasmid pET-21a containing the α-synuclein (aSYN) gene was used as a template for site-directed mutagenesis. Primers were designed to introduce specific mutations at positions A30P, A53T, E46K and H50Q. A30P: Forward: AGCACCAGGAAAGACAAAAGAGG; Reversed: TTCC TGGTGCTTCTGCCACACCC; A53T: Forward: TGTGA CAACAGTGGCTGAGAAG; Reversed: GTTGTCACAC CATGCACCACTC; E46K: Forward: CAAGAAGGGAG TGGTGCATGGTG; Reversed: CTCCCTTCTTGGTTTT GGAGCCT; H50Q: Forward: GGTGCAAGGTGTGG CAACAG; Reversed: CACCTTGCACCACTCCCTCC. PCR reactions (50 μL) were performed using 50 ng of plasmid template, 2 mM of each primer, 200 μM dNTPs, and 2 U of DNA fusion polymerase. The amplification products were analysed by 1% agarose gel electrophoresis, purified using the PureLink™ PCR Purification Kit (Thermo Fisher Scientific, Waltham, MA, USA), and subsequently treated with DpnI (NEB) to degrade the template DNA. Following digestion, 5 μL of the purified PCR product was transformed into DH5α competent E. coli cells and plated on Luria–Bertani (LB) agar, containing 100 $\mu g \cdot mL^{-1}$ ampicillin. Ten colonies were selected, and their plasmids were extracted using the Thermo Fisher Scientific miniprep kit. Mutants were initially screened by NdeI and XhoI restriction digestion, and successful mutants were confirmed by Sanger sequencing (Eurofins).

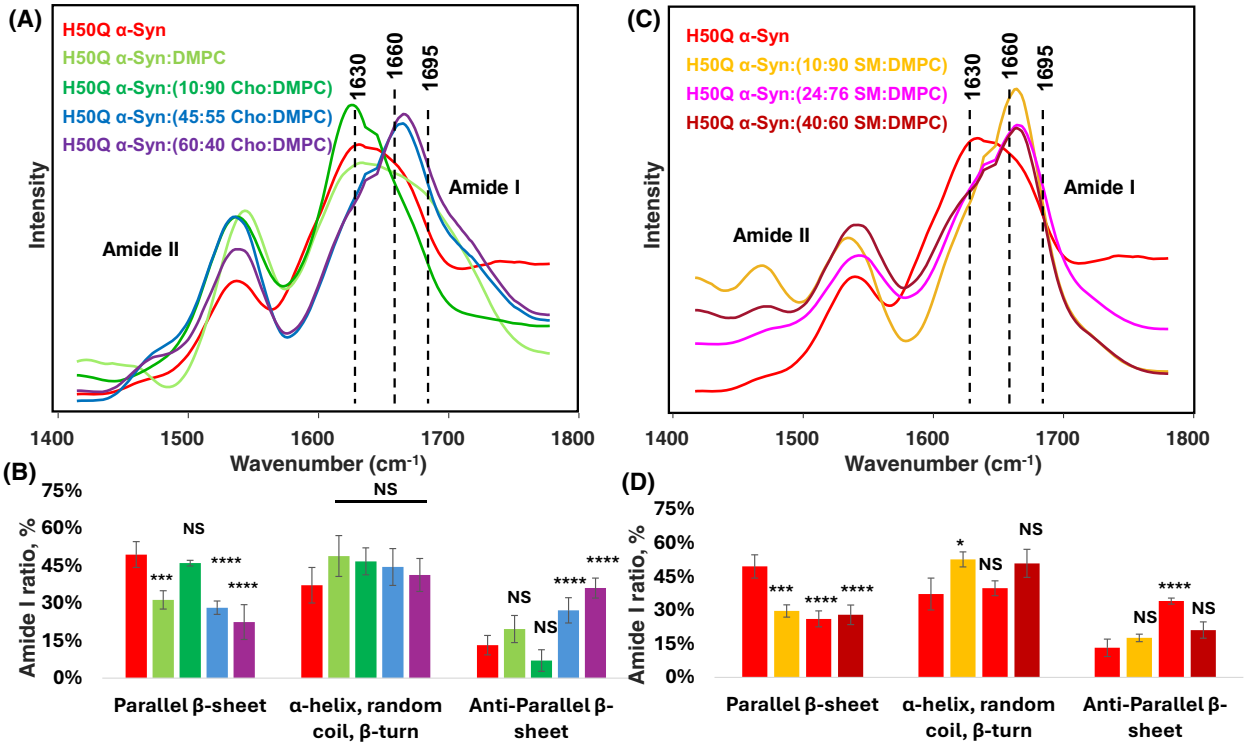

Fig. 13. Influence of lipids on the secondary structure of α-syn aggregates. Atomic force microscopy Infrared spectra (A and C) and histograms (B and D) showing the amount of parallel β-sheet, α-helix, random coil, and β-turn, as well as antiparallel β-sheet in the secondary structure of H50Q α-syn aggregates-grown presence of LUVs with different concentrations of 1,2-dimyristoyl-sn-glycero-3-phosphatidylcholine (DMPC), cholesterol (Cho) and sphingomyelin (SM), as well as in the lipid-free environment. Lipid-free conditions are in red; DMPC in light green, (10:90 Cho:DMPC) in green, (45:55 Cho:DMPC) in blue, (60:40 Cho:DMPC) in purple, (10:90 SM:DMPC) in yellow, (24:76 SM:DMPC) in pink, and (40:60 SM:DMPC) in maroon. Each curve shown in panels A–C is the average of three sample replicates ($n = 3$). The graphical data are presented as the mean ± SEM. According to one-way ANOVA followed by Tukey's HSD test, $*P < 0.05$, $***P < 0.001$, **** < 0.0001. NS shows the absence of statistically significant differences.

Overexpression and initial purification of α-Syn and α-Syn mutants (A30P, A53T, E46K, and H50Q)

The pET21a-α-synuclein plasmid, along with its mutants (A30P, A53T, E46K, and H50Q), was overexpressed in *Escherichia coli* BL21 (DE3) Rosetta cells using LB broth, following the protocol described by Volles and Lansbury [52]. A two-litre bacterial culture was induced with 1 mM IPTG, grown to the desired density, and harvested by centrifugation at 8000 RPM for 10 min. The resulting cell pellet was resuspended in a lysis buffer (50 mM Tris, 10 mM EDTA, 150 mM NaCl, pH 7.5), supplemented with a protease inhibitor cocktail (Roche (Hoffmann-La Roche AG), Basel, Switzerland). Lysis was performed by two freeze–thaw cycles, followed by sonication. The lysate was then heated in a water bath at 100 °C for 30 min to denature unwanted proteins.

After heat treatment, the sample was centrifuged at 16 000 ***g*** for 30 min and the supernatant was collected. To remove nucleic acids and contaminants, 10% streptomycin sulfate (136 $\mu L \cdot mL^{-1}$) and glacial acetic acid (228 $\mu L \cdot mL^{-1}$) were added, followed by centrifugation at 16 000 ***g*** for 10 min at 4 °C. The resulting supernatant was subjected to protein precipitation by adding an equal volume of saturated ammonium sulfate at 4 °C. The precipitate was washed with a 1:1 (v/v) mixture of saturated ammonium sulfate and water at 4 °C, then resuspended in 100 mM ammonium acetate (NH_4CH_3COO) under constant stirring for 10 min. To further purify the protein, absolute ethanol precipitation was performed twice at room temperature. The collected protein pellet was resuspended in 100 mM ammonium acetate, lyophilised, and stored at −20 °C for subsequent chromatographic purification.

Gel filtration chromatography of expressed proteins

Proteins were dissolved in PBS buffer, pH 7.4 and centrifuged for 30 min at 14 000 ***g*** using a benchtop microcentrifuge (Eppendorf centrifuge 5424, USA). Next, 500 µL of concentrated protein was loaded on a Superdex 200 10/300 gel filtration column in AKTA pure (GE Healthcare Technologies Inc., Chicago, IL, USA) FPLC. Proteins were eluted

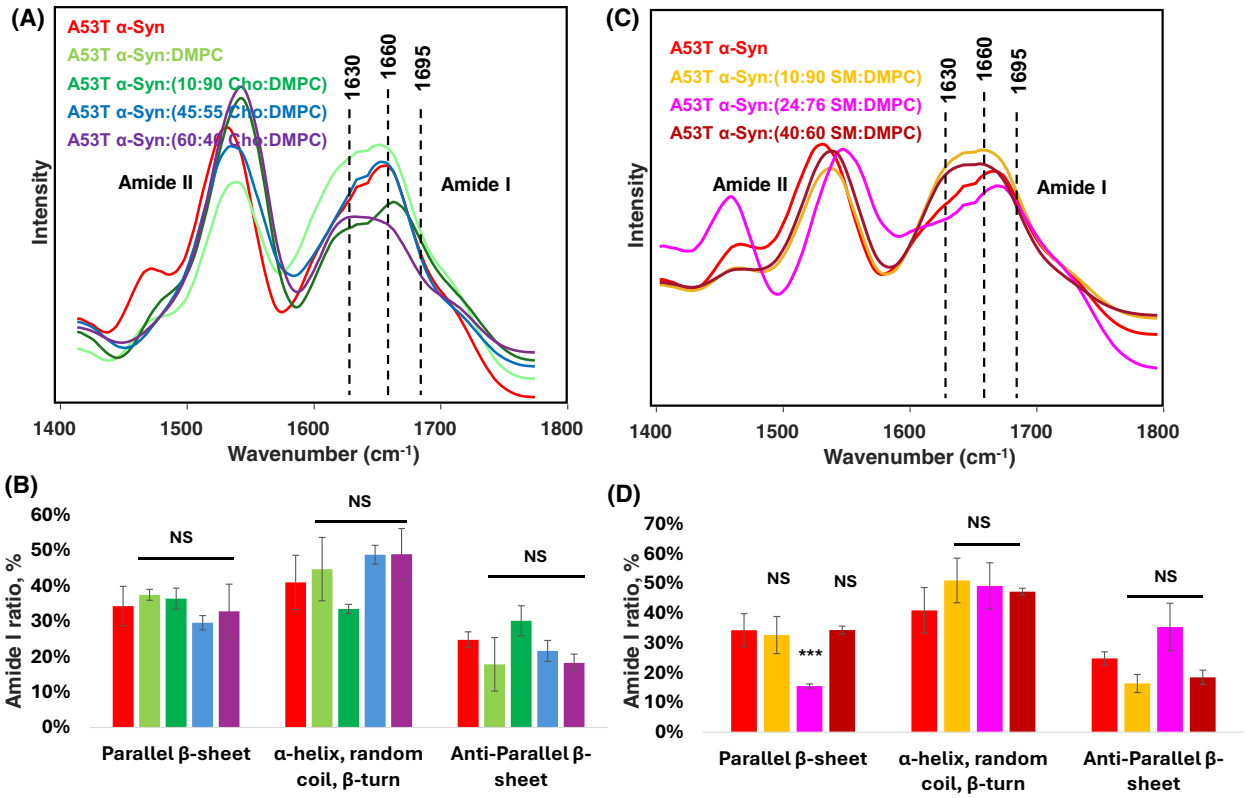

Fig. 14. Influence of lipids on the secondary structure of α-syn aggregates. AFM-IR spectra (A and C) and histograms (B and D) showing the amount of parallel β-sheet, α-helix, random coil, and β-turn, as well as antiparallel β-sheet in the secondary structure of A53T α-syn aggregates-grown presence of LUVs with different concentrations of 1,2-dimyristoyl-sn-glycero-3-phosphatidylcholine (DMPC), cholesterol (Cho) and sphingomyelin (SM), as well as in the lipid-free environment. Lipid-free conditions are in red; DMPC in light green, (10:90 Cho:DMPC) in green, (45:55 Cho:DMPC) in blue, (60:40 Cho:DMPC) in purple, (10:90 SM:DMPC) in yellow, (24:76 SM:DMPC) in pink, and (40:60 SM:DMPC) in maroon. Each curve shown in panels A–C is the average of three sample replicates ($n = 3$). The graphical data are presented as the mean ± SEM. According to one-way ANOVA followed by Tukey's HSD test, ***$P < 0.001$. NS shows the absence of statistically significant differences.

isocratically with a flow rate of 0.5 mL·min^{-1} at 4 °C using the same buffer and 1.5 mL fractions were collected according to the UV–VIS detection at 280 nm.

Preparation of large unilamellar vesicles (LUVs)

Vesicles composed of DMPC, 10:90 Cho:DMPC, 45:55 Cho:DMPC, 60:40 Cho:DMPC, 10:90 SM:DMPC, 24:76 SM:DMPC and 40:60 SM:DMPC were prepared following the method described by Galvagnion et al. [11]. First, individual lipids and their mixtures were dissolved in phosphate-buffered saline (PBS, pH 7.4). The lipid suspensions were then heated in a water bath at ~65 °C for 30 min to ensure proper hydration. Next, the samples were rapidly frozen in liquid nitrogen for 1 min. This freeze–thaw cycle was repeated 8–10 times to promote vesicle formation. Finally, the suspensions were extruded through a 100 nm membrane using an Avanti extruder (Alabaster, AL, USA) to obtain uniformly sized LUVs.

Protein aggregation

In a lipid-free environment, 100 μM of α-syn and α-syn mutants (A30P, A53T, E46K and H50Q) were dissolved in PBS (pH 7.4). For lipid-containing conditions, 100 μM of α-synuclein, A30P, A53T, E46K and H50Q were mixed with an equimolar concentration of DMPC, 10:90 Cho:DMPC, 45:55 Cho:DMPC, 60:40 Cho:DMPC, 10:90 SM:DMPC, 24:76 SM:DMPC or 40:60 SM:DMPC. The final pH of the solutions was adjusted to 7.4 using concentrated HCl. Next, samples were transferred into a 96-well plate and incubated in a Tecan plate reader (Männedorf, Switzerland) at 37 °C for 160 h under 510 rpm agitation.

Thioflavin T (ThT) assay

Protein aggregation rates were monitored using a Thioflavin T (ThT) fluorescence assay. For this, samples were mixed with 2 mM ThT solution and transferred into a 96-

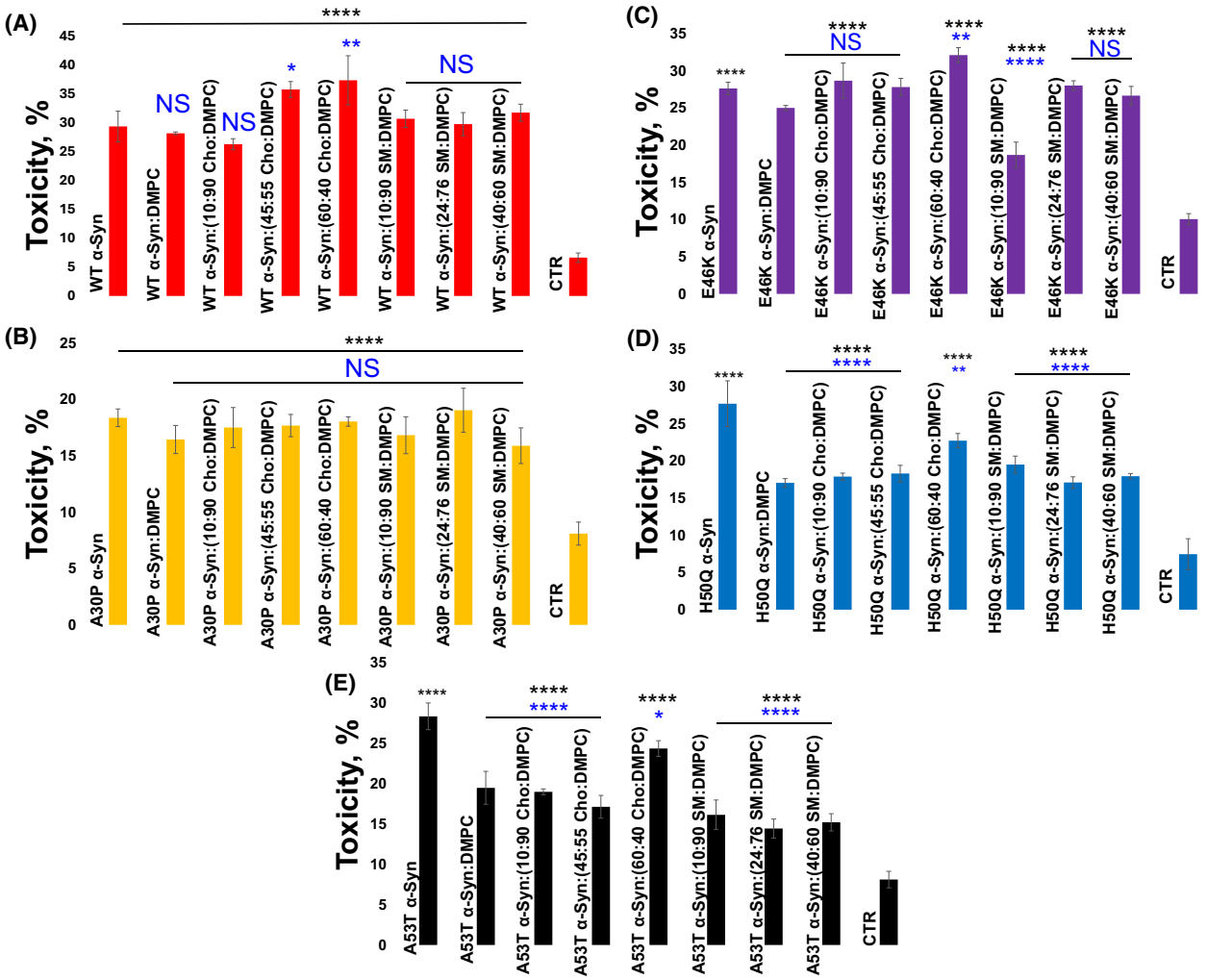

Fig. 15. Influence of lipids on the cytotoxicity of α-syn aggregates. Histograms of lactate dehydrogenase assay of WT α-syn, A30P, E46K, H50Q, and A53T α-syn fibrils-grown presence of large unilamellar vesicles with different concentrations of 1,2-dimyristoyl-sn-glycero-3-phosphatidylcholine (DMPC), cholesterol (Cho) and sphingomyelin (SM), as well as in the lipid-free environment. All measurements were made in triplicates. Means of three replicates are shown in the figures. At least two independent experiments were made for each set of samples. One-way ANOVA with Tukey's honestly significant difference *post hoc* was performed to reveal statistical significance between samples relative to control (ctr) (black) and fibrils with no lipids (blue). The graphical data are presented as the mean ± SEM. NS is a nonsignificant difference; $*P \leq 0.05$, $**P \leq 0.01$, and $****P \leq 0.0001$.

well plate. The plate was incubated in a Tecan plate reader (Männedorf, Switzerland) at 37 °C for 160 h under continuous agitation at 510 rpm. Fluorescence readings were recorded every 10 min with an excitation wavelength of 450 nm and an emission wavelength of 488 nm. Each kinetic curve represents the average of three independent experiments. To calculate the lag-phase (t_{lag}) and half-time ($t_{1/2}$) of protein aggregation, time points at which the ThT intensity was 10% and 50% of the maximal plateau values were taken and reported in Figs 1–3. A dip in the plateau phase in several cases is likely to be caused by precipitation of the formed protein aggregates to the bottom of the plastic well, which is common for plate-reader-based ThT measurements [30,53]. It should be noted that in the absence of the protein, LUVs themselves give no changes in the ThT signal.

Atomic force microscopy and atomic force microscopy-infrared spectroscopy (AFM-IR)

Microscopic analysis of α-syn and α-syn mutants aggregates was performed using Nano-IR3 system (Bruker, Santa Barbara, CA, USA). Samples were diluted 1:15 in deionised (DI) water before deposition on gold-coated

silicon wafer. For each sample, three 10 × 10 μm areas were scanned, with 6–7 height measurements recorded from each region before capturing the final image. Imaging and spectral acquisition were performed using gold-coated contact-mode AFM probes (ContGB-G, Nano-AndMore, Watsonville, CA, USA). Each spectrum was collected three times, averaged, and smoothed using a Savitzky–Golay filter (second order) in MATLAB. Spectral deconvolution of the averaged spectra was performed in GRAMS/AI. Secondary structure assignments were based on characteristic absorption bands: parallel β-sheet at 1624 cm^{-1}, α-helix and random coil at 1655 cm^{-1}, β-turn at 1682 cm^{-1}, and anti-parallel β-sheet at 1698 cm^{-1}.

Circular dichroism (CD) spectroscopy

After 150 h of aggregation, samples were diluted with PBS and transferred into a quartz cuvette. CD spectra were recorded immediately using a Jasco J-1000 CD spectrometer (Jasco, Easton, MD, USA). For each sample, three spectra were collected over the wavelength range of 190–240 nm and subsequently averaged to ensure accuracy.

Attenuated total reflectance Fourier-transform infrared (ATR-FTIR) spectroscopy

Samples were first deposited onto the ATR crystal of a PerkinElmer 100 FTIR spectrometer (Waltham, MA, USA), equipped with an ATR module. Samples were air-dried at room temperature before spectral acquisition. For each sample, three spectra were recorded and averaged to ensure accuracy.

Cell toxicity assay on N27 rat dopaminergic neurons

N27 cells (MilliporeSigma, Burlington, MA, USA; cat. no. SCC048, RRID:CVCL_D584) were cultured in 96-well plates with RPMI 1640 medium supplemented with 10% fetal bovine serum (FBS) at 37 °C and 5% CO_2. N27 cell line is not listed as commonly misidentified by ICLAC. The cells were not authenticated post-purchase and were used for a maximum of 10 passages. All experiments were performed with mycoplasma-free cells. Once the cells reached approximately 70% confluency after 24 h of incubation, they were ready for experimentation. For the LDH assay, 100 μL of the medium was replaced with fresh RPMI 1640 medium containing 5% FBS, and 10 μL of the protein sample was added. The reduction in FBS concentration was done to minimise baseline absorbance in the samples. After an additional 24 h of incubation, the CytoTox 96® Non-Radioactive Cytotoxicity Assay Kit (G1781, Promega, Madison, WI, USA) was used to quantify the amount of lactate dehydrogenase (LDH) released into the culture medium.

Acknowledgement

We are grateful to the National Institute of Health for the provided financial support (R35GM142869).

Conflict of interest

The authors declare no competing financial interests.

Author contributions

AA performed experiments, analysed and visualised results, edited the manuscript; MM performed cytotoxicity assays; analysed results, edited the manuscript; DK conceptualised and supervised the study, acquired finding, visualised results, wrote and edited the manuscript.

Peer review

The peer review history for this article is available at https://www.webofscience.com/api/gateway/wos/peer-review/10.1111/febs.70363.

Data availability statement

All data described in this manuscript are contained within the manuscript.

References

1 Krack P, Volkmann J, Tinkhauser G & Deuschl G (2019) Deep brain stimulation in movement disorders: from experimental surgery to evidence-based therapy. *Mov Disord* **34**, 1795–1810.
2 Hoffmann AC, Minakaki G, Menges S, Salvi R, Savitskiy S, Kazman A, Vicente Miranda H, Mielenz D, Klucken J, Winkler J *et al.* (2019) Extracellular aggregated alpha synuclein primarily triggers lysosomal dysfunction in neural cells prevented by trehalose. *Sci Rep* **9**, 544.
3 Vogiatzi T, Xilouri M, Vekrellis K & Stefanis L (2008) Wild type alpha-synuclein is degraded by chaperone-mediated autophagy and macroautophagy in neuronal cells. *J Biol Chem* **283**, 23542–23556.
4 Chen J (2010) Parkinson's disease: health-related quality of life, economic cost, and implications of early treatment. *J Am J Manag Care* **16**, S87–S93.
5 Hawkes CH, Del Tredici K & Braak H (2007) Parkinson's disease: a dual-hit hypothesis. *Neuropathol Appl Neurobiol* **33**, 599–614.
6 Braak H, Del Tredici K, Rub U, de Vos RA, Jansen Steur EN & Braak E (2003) Staging of brain pathology related to sporadic Parkinson's disease. *Neurobiol Aging* **24**, 197–211.

7 Braak H, Ghebremedhin E, Rub U, Bratzke H & Del Tredici K (2004) Stages in the development of Parkinson's disease-related pathology. *Cell Tissue Res* **318**, 121–134.

8 Shahmoradian SH, Lewis AJ, Genoud C, Hench J, Moors TE, Navarro PP, Castano-Diez D, Schweighauser G, Graff-Meyer A, Goldie KN *et al.* (2019) Lewy pathology in Parkinson's disease consists of crowded organelles and lipid membranes. *Nat Neurosci* **22**, 1099–1109.

9 Dou T, Matveyenka M & Kurouski D (2023) Elucidation of secondary structure and toxicity of alpha-Synuclein oligomers and fibrils grown in the presence of phosphatidylcholine and phosphatidylserine. *ACS Chem Neurosci* **14**, 3183–3191.

10 Galvagnion C (2017) The role of lipids interacting with -Synuclein in the pathogenesis of Parkinson's disease. *J Parkinsons Dis* **7**, 433–450.

11 Galvagnion C, Brown JW, Ouberai MM, Flagmeier P, Vendruscolo M, Buell AK, Sparr E & Dobson CM (2016) Chemical properties of lipids strongly affect the kinetics of the membrane-induced aggregation of alpha-synuclein. *Proc Natl Acad Sci U S A* **113**, 7065–7070.

12 Galvagnion C, Buell AK, Meisl G, Michaels TC, Vendruscolo M, Knowles TP & Dobson CM (2015) Lipid vesicles trigger alpha-synuclein aggregation by stimulating primary nucleation. *Nat Chem Biol* **11**, 229–234.

13 Chen SW, Drakulic S, Deas E, Ouberai M, Aprile FA, Arranz R, Ness S, Roodveldt C, Guilliams T, De-Genst EJ *et al.* (2015) Structural characterization of toxic oligomers that are kinetically trapped during alpha-synuclein fibril formation. *Proc Natl Acad Sci U S A* **112**, E1994–E2003.

14 Dou T & Kurouski D (2022) Phosphatidylcholine and phosphatidylserine uniquely modify the secondary structure of alpha-Synuclein oligomers formed in their presence at the early stages of protein aggregation. *ACS Chem Neurosci* **13**, 2380–2385.

15 Matveyenka M, Ali A, Mitchell CL, Sholukh M & Kurouski D (2024) Elucidation of cytotoxicity of alpha-Synuclein fibrils on immune cells. *Biochim Biophys Acta Proteins Proteomics* **1873**, 141061.

16 Hannestad JK, Rocha S, Agnarsson B, Zhdanov VP, Wittung-Stafshede P & Hook F (2020) Single-vesicle imaging reveals lipid-selective and stepwise membrane disruption by monomeric alpha-synuclein. *Proc Natl Acad Sci U S A* **117**, 14178–14186.

17 Middleton ER & Rhoades E (2010) Effects of curvature and composition on alpha-synuclein binding to lipid vesicles. *Biophys J* **99**, 2279–2288.

18 van Rooijen BD, Claessens MM & Subramaniam V (2009) Lipid bilayer disruption by oligomeric alpha-synuclein depends on bilayer charge and accessibility of the hydrophobic core. *Biochim Biophys Acta* **1788**, 1271–1278.

19 Iyer A & Claessens M (2019) Disruptive membrane interactions of alpha-synuclein aggregates. *Biochimica et Biophysica Acta (BBA)* **1867**, 468–482.

20 Iyer A, Petersen NO, Claessens MM & Subramaniam V (2014) Amyloids of alpha-synuclein affect the structure and dynamics of supported lipid bilayers. *Biophys J* **106**, 2585–2594.

21 Iyer A, Roeters SJ, Schilderink N, Hommersom B, Heeren RM, Woutersen S, Claessens MM & Subramaniam V (2016) The impact of N-terminal acetylation of alpha-Synuclein on phospholipid membrane binding and fibril structure. *J Biol Chem* **291**, 21110–21122.

22 Iyer A, Schilderink N, Claessens M & Subramaniam V (2016) Membrane-bound alpha Synuclein clusters induce impaired lipid diffusion and increased lipid packing. *Biophys J* **111**, 2440–2449.

23 Stockl M, Fischer P, Wanker E & Herrmann A (2008) Alpha-Synuclein selectively binds to anionic phospholipids embedded in liquid-disordered domains. *J Mol Biol* **375**, 1394–1404.

24 Matveyenka M, Ali A, Mitchell CL, Brown HC & Kurouski D (2024) Cholesterol accelerates aggregation of alpha-Synuclein simultaneously increasing the toxicity of amyloid fibrils. *ACS Chem Neurosci* **15**, 4075–4081.

25 Ali A, Holman AP, Rodriguez A, Osborne L & Kurouski D (2024) Elucidating the mechanisms of alpha-Synuclein-lipid interactions using site-directed mutagenesis. *Neurobiol Dis* **198**, 106553.

26 Farid I, Ali A, Holman AP, Osborne L & Kurouski D (2024) Length and saturation of choline plasmalogens alter the aggregation rate of alpha-synuclein but not the toxicity of amyloid fibrils. *Int J Biol Macromol* **264**, 130632.

27 Flagmeier P, Meisl G, Vendruscolo M, Knowles TP, Dobson CM, Buell AK & Galvagnion C (2016) Mutations associated with familial Parkinson's disease alter the initiation and amplification steps of alpha-synuclein aggregation. *Proc Natl Acad Sci U S A* **113**, 10328–10333.

28 Ali A, Zhaliazka K, Dou T, Holman AP & Kurouski D (2023) The toxicities of A30P and A53T alpha-synuclein fibrils can be uniquely altered by the length and saturation of fatty acids in phosphatidylserine. *J Biol Chem* **299**, 105383.

29 Holman AP, Pickett DN, Orr AE, Tarone AM & Kurouski D (2024) A nondestructive technique for the sex identification of third instar *Cochliomyia macellaria* larvae. *J Forensic Sci* **69**, 2075–2081.

30 Ali A, Zhaliazka K, Dou T, Holman AP & Kurouski D (2023) Cholesterol and sphingomyelin uniquely Alter the rate of transthyretin aggregation and decrease the toxicity of amyloid fibrils. *J Phys Chem Lett* **14**, 10886–10893.

31 Dazzi A & Prater CB (2017) AFM-IR: technology and applications in nanoscale infrared spectroscopy and chemical imaging. *Chem Rev* **117**, 5146–5173.
32 Centrone A (2015) Infrared imaging and spectroscopy beyond the diffraction limit. *Annu Rev Anal Chem* **8**, 101–126.
33 Ramer G, Ruggeri FS, Levin A, Knowles TPJ & Centrone A (2018) Determination of polypeptide conformation with nanoscale resolution in water. *ACS Nano* **12**, 6612–6619.
34 Ruggeri FS, Flagmeier P, Kumita JR, Meisl G, Chirgadze DY, Bongiovanni MN, Knowles TPJ & Dobson CM (2020) The influence of pathogenic mutations in alpha-Synuclein on biophysical and structural characteristics of amyloid fibrils. *ACS Nano* **14**, 5213–5222.
35 Ruggeri FS, Longo G, Faggiano S, Lipiec E, Pastore A & Dietler G (2015) Infrared nanospectroscopy characterization of oligomeric and fibrillar aggregates during amyloid formation. *Nat Commun* **6**, 7831.
36 Zhaliazka K, Ali A & Kurouski D (2024) Phospholipids and cholesterol determine molecular mechanisms of cytotoxicity of alpha-Synuclein oligomers and fibrils. *ACS Chem Nerosci* **15**, 371–381.
37 Alecu I & Bennett SAL (2019) Dysregulated lipid metabolism and its role in alpha-Synucleinopathy in Parkinson's disease. *Front Neurosci* **13**, 328.
38 Walsh DM, Klyubin I, Fadeeva JV, Cullen WK, Anwyl R, Wolfe MS, Rowan MJ & Selkoe DJ (2002) Naturally secreted oligomers of amyloid beta protein potently inhibit hippocampal long-term potentiation in vivo. *Nature* **416**, 535–539.
39 Vilar M, Chou HT, Luhrs T, Maji SK, Riek-Loher D, Verel R, Manning G, Stahlberg H & Riek R (2008) The fold of alpha-synuclein fibrils. *Proc Natl Acad Sci USA* **105**, 8637–8642.
40 Heise H, Hoyer W, Becker S, Andronesi OC, Riedel D & Baldus M (2005) Molecular-level secondary structure, polymorphism, and dynamics of full-length alpha-synuclein fibrils studied by solid-state NMR. *Proc Natl Acad Sci USA* **102**, 15871–15876.
41 Kurouski D, Luo H, Sereda V, Robb FT & Lednev IK (2013) Deconstruction of stable cross-Beta fibrillar structures into toxic and nontoxic products using a mutated archaeal chaperonin. *ACS Chem Biol* **8**, 2095–2101.
42 Singh Y, Sharpe PC, Hoang HN, Lucke AJ, McDowall AW, Bottomley SP & Fairlie DP (2011) Amyloid formation from an alpha-helix peptide bundle is seeded by 3(10)-helix aggregates. *Chem* **17**, 151–160.
43 Viennet T, Wordehoff MM, Uluca B, Poojari C, Shaykhalishahi H, Willbold D, Strodel B, Heise H, Buell AK, Hoyer W *et al.* (2018) Structural insights from lipid-bilayer nanodiscs link alpha-Synuclein membrane-binding modes to amyloid fibril formation. *Commun Biol* **1**, 44.
44 Giasson BI, Murray IV, Trojanowski JQ & Lee VM (2001) A hydrophobic stretch of 12 amino acid residues in the middle of alpha-synuclein is essential for filament assembly. *J Biol Chem* **276**, 2380–2386.
45 Dam T, Chouliara M, Junghans V & Jonsson P (2022) Supported lipid bilayers and the study of two-dimensional binding kinetics. *Front Mol Biosci* **9**, 833123.
46 Alza NP, Iglesias Gonzalez PA, Conde MA, Uranga RM & Salvador GA (2019) Lipids at the crossroad of alpha-Synuclein function and dysfunction: biological and pathological implications. *Front Cell Neurosci* **13**, 175.
47 Jo E, Fuller N, Rand RP, St George-Hyslop P & Fraser PE (2002) Defective membrane interactions of familial Parkinson's disease mutant A30P alpha-synuclein. *J Mol Biol* **315**, 799–807.
48 Perlmutter JD, Braun AR & Sachs JN (2009) Curvature dynamics of alpha-synuclein familial Parkinson disease mutants: molecular simulations of the micelle- and bilayer-bound forms. *J Biol Chem* **284**, 7177–7189.
49 McClain SM, Ojoawo AM, Lin W, Rienstra CM & Murphy CJ (2020) Interaction of alpha-Synuclein and its mutants with rigid lipid vesicle mimics of varying surface curvature. *ACS Nano* **14**, 10153–10167.
50 Ali A, Holman AP, Rodriguez A, Matveyenka M & Kurouski D (2024) Tubulin-binding region alters tau-lipid interactions and changes toxicity of tau fibrils formed in the presence of phosphatidylserine lipids. *Protein Sci* **33**, e5078.
51 Ali A, Matveyenka M, Pickett DN, Rodriguez A & Kurouski D (2025) Tubulin-binding region modulates cholesterol-triggered aggregation of tau proteins. *J Neurochem* **169**, e16294.
52 Volles MJ & Lansbury PT Jr (2007) Relationships between the sequence of alpha-synuclein and its membrane affinity, fibrillization propensity, and yeast toxicity. *J Mol Biol* **366**, 1510–1522.
53 Holman AP, Dou T, Matveyenka M, Zhaliazka K, Patel A, Maalouf A, Elsaigh R & Kurouski D (2025) The role of phospholipid saturation and composition in alpha-synuclein aggregation and toxicity: a dual in vitro and in vivo approach. *Protein Sci* **34**, e70121.

Supporting information

Additional supporting information may be found online in the Supporting Information section at the end of the article.

Table S1. Height (Z) values of AFM images.